



Cite this: DOI: 10.1039/d4su00098f

## Unlocking sustainable power: advances in aqueous processing and water-soluble binders for NMC cathodes in high-voltage Li-ion batteries

Ana Clara Rolandi,<sup>abc</sup> Iratxe de Meatza,<sup>b</sup> Nerea Casado,<sup>cd</sup> Maria Forsyth,<sup>ad</sup> David Mecerreyes<sup>cd</sup> and Cristina Pozo-Gonzalo<sup>aeef</sup>

Current cathode electrode processing of lithium-ion batteries relies on the conventional use of polyvinylidene fluoride (PVDF) as a binder, accompanied by the toxic solvent *N*-methylpyrrolidone (NMP). Within cathode materials, the  $\text{LiNi}_x\text{Mn}_{1-x-y}\text{Co}_y\text{O}_2$  (NMC) families stand out as most promising candidates for the next generation of lithium-ion batteries, boasting high energy density and capacity. This review extensively compares traditional battery manufacturing methods with the use of emerging waterborne binders, highlighting the benefits in terms of cost-effectiveness, environmental sustainability, and enhanced processing conditions. The transition to sustainable aqueous processing encounters challenges, including pH elevation, aluminium collector corrosion, and lithium leaching from the NMC materials. The exploration extends to tailored binder selection and additives, crucial in optimizing electrochemical properties for distinct NMC compositions, such as  $\text{LiNi}_{0.33}\text{Mn}_{0.33}\text{Co}_{0.33}\text{O}_2$  (NMC 111),  $\text{LiNi}_{0.5}\text{Mn}_{0.3}\text{Co}_{0.2}\text{O}_2$  (NMC 532),  $\text{LiNi}_{0.6}\text{Mn}_{0.2}\text{Co}_{0.2}\text{O}_2$  (NMC 622) and  $\text{LiNi}_{0.8}\text{Mn}_{0.1}\text{Co}_{0.1}\text{O}_2$  (NMC 811), and addressing challenges inherent in their aqueous processing. The integration of aqueous binders promises advancements and also shapes a strategic outlook for future research, contributing significantly to the sustainability of lithium-ion batteries.

Received 26th February 2024  
Accepted 8th June 2024

DOI: 10.1039/d4su00098f

rsc.li/rscsus

<sup>a</sup>Institute for Frontier Materials, Deakin University, Melbourne 3125, Australia<sup>b</sup>CIDETEC Basque Research and Technology Alliance (BRTA), 20014 Donostia-San Sebastian, Spain<sup>c</sup>POLYMAT, University of the Basque Country UPV/EHU, Donostia-San Sebastián 20018, Spain. E-mail: david.mecerreyes@ehu.es<sup>d</sup>IKERBASQUE, Basque Foundation for Science, Bilbao 48011, Spain<sup>e</sup>Fundación Agencia Aragonesa para la Investigación y el Desarrollo (ARAID), Av. de Ranillas 1-D, 50018 Zaragoza, Spain<sup>f</sup>Instituto de Carboquímica (ICB-CSIC), C/Miguel Luesma Castán, 4, 50018, Zaragoza, Spain. E-mail: cpozo@csic.es

Ana Clara Rolandi

energy solutions and innovative battery technology are among her primary research interests.

Ana Clara Rolandi completed her degree in Materials Engineering at the National University of Mar del Plata, Argentina, in 2020. She is currently pursuing a cotutelle PhD between the Basque Country University in Spain and Deakin University in Australia. Her research focuses on investigating water-soluble binders for high-voltage cathodes in lithium-ion batteries, aiming to replace toxic organic solvents. Sustainable



Iratxe de Meatza

formulations and processing optimization, full cell harmonization, electrochemical characterization, cell prototyping) since 2004. She has participated in 20+ EU projects on batteries and is co-author of more than 45 SCI papers (H-index = 21) and 1 patent on aqueous cathode processing.

Iratxe de Meatza is Research Scientist and Project Manager at CIDETEC Energy Storage, currently Team Leader on Advanced Li-ion batteries. Born on 1977 in Bilbao (Basque Country, Spain), studied Chemistry with postgraduate focus on Inorganic Materials (PhD at University of the Basque Country), working initially on perovskite-type oxides for solid oxide fuel cells. She has focused on lithium batteries (electrode



### Sustainability spotlight

SDG7: affordable and clean energy – aqueous processing of high-voltage cathodes provides a promising path for reducing the carbon footprint of overall cell production. By reducing production costs, potentially incorporating biosourced polymers, and simplifying the recovery of active materials during battery recycling, this approach presents a comprehensive solution towards sustainable battery technology. SDG13: climate action – by employing water as the solvent for electrode processing, we can mitigate potential environmental and occupational hazards by eliminating the need for toxic *N*-methylpyrrolidone (NMP) solvent. Utilising water allows for lower drying temperatures for electrodes, resulting in additional energy savings. Moreover, substituting fluorinated polymers enhances the sustainability of batteries, as these polymers pose challenges in disposal.

## 1 Introduction

In the contemporary era, addressing the consequences of climate change and establishing an economy based on sustainable energy is a compelling societal necessity. In June 2021, the European Union committed to achieving net-zero

greenhouse gas emissions by 2050 through the European Climate Law.<sup>1,2</sup> The combustion of fossil fuels, primarily releasing CO<sub>2</sub>, contributes to the well-acknowledged global warming phenomenon.<sup>3</sup> The challenge is exacerbated by the dominance of fossil fuels in the world's energy supply, coupled with escalating global development fuelling society's energy



**Nerea Casado**

*Nerea Casado is an Ikerbasque Research Fellow at POLYMAT, University of the Basque Country in Spain. Her research interests include the design of new redox polymers and binders for energy including batteries and hydrogen energy devices. She has published over 40 articles and co-edited one book on these topics.*



**Maria Forsyth**

*Maria Forsyth AM ATSE (Australian Academy of Technology and Engineering), FAA (Fellow Australian Academy of Sciences), is an Alfred Deakin Professorial Fellow at Deakin University and an Ikerbasque Visiting Professorial Fellow at University of the Basque Country, Spain. She has worked at the forefront of energy materials research since her Fulbright Research Fellowship in 1990 and has consistently made*

*breakthrough discoveries in next-generation lithium and sodium battery technologies. She has supervised over 100 PhD students and is a coauthor of over 780 journal and conference publications.*



**David Mecerreyes**

*David Mecerreyes is an Ikerbasque Research Professor at POLYMAT, University of the Basque Country in Spain. His actual research interests include the design of new polymers for applications in emerging technologies in energy, the environment, and bioelectronics. He has published over 400 peer-reviewed articles. He is an associate editor of the journal ACS Applied Polymer Materials and a member of the Advisory Board of ACS Macro Letters.*



**Cristina Pozo-Gonzalo**

*A/Prof. Pozo-Gonzalo is an ARAID Fellow, working at the Carboquímica Institute (Spain) and an honorary Associate Professor at Deakin University (Melbourne). She received her PhD degree in from the University of Manchester (United Kingdom) on the electrochemical synthesis of conducting polymers. Her current research interest focuses on energy, working on the recovery of critical raw materials from waste using safe and unexpensive methods, and redesign of materials for energy. During her research career, she has authored and co-authored 106 peer-review international publications, 3 book chapters and holds 4 patents, in the areas of electrochemistry, materials, circular economy and energy storage.*



demands. Worldwide consensus has emerged around the imperative to decarbonise transportation infrastructure. A promising path for more sustainable electrochemical energy storage are secondary batteries and double-layer capacitors.<sup>4,5</sup> Due to their high energy density, prolonged cycle life and lightweight composition, lithium-ion batteries (LIBs) emerged as ideal power sources for compact spaces, powering an array of portable electronic devices and enabling technological innovation. The reliability of LIBs makes them indispensable nowadays, ensuring the continuous operation of consumer electronics and critical medical devices, emphasizing their extensive impact on our daily lives and overall societal well-being.<sup>6</sup> Due to their portability, versatility and efficiency, LIBs find extensive use in various electronic devices.<sup>7</sup>

Persistent efforts have been dedicated to improving LIBs performance, with a primary emphasis on the innovation of new active materials and electrolytes.<sup>8,9</sup> Recently, there has been a surge in attention towards the binder, despite its relatively modest mass contribution (2–5 wt%) in the electrode preparation.<sup>10,11</sup> The binder serves a dual function in facilitating adhesion between active materials and conductive additives,<sup>12</sup> binding them onto metal current collectors, and fostering cohesion within the electrode structure, thus enabling efficient electrochemical reactions.<sup>13</sup> Current battery electrode processing technologies employ polyvinylidene fluoride (PVDF) as binder,<sup>10</sup> which requires the use of the toxic *N*-methyl-2-pyrrolidone (NMP) as a solvent. Since NMP is a hazardous, teratogenic, and irritating compound,<sup>14,15</sup> new environmentally friendly solvent for electrode processing, such as water, is indispensable. During the battery recycling process, the water-soluble binders will facilitate the separation of the active materials from the current collector by direct immersion of the whole electrode in water.<sup>16–18</sup> On the other hand, the removal of PVDF is difficult since it is a hydrophobic and chemically stable fluorinated polymer.<sup>16</sup> While thermal treatment stands out as a direct method for liberating electroactive materials from PVDF, their drawbacks, including the release of hazardous products (including hydrogen fluoride gas and fluoride hydrocarbons such as vinylidene fluoride and trifluoro benzene)<sup>19,20</sup> and high energy consumption (500 to 700 °C pyrolysis temperature range) compromise the sustainability and economic viability of battery recycling.<sup>18,21</sup> Therefore, issues such as scarcity of valuable metals or groundwater and soil contamination by landfill accumulation of spent LIBs can be lessened by the use of water-soluble binders.<sup>22</sup>

Apart from  $\text{LiFePO}_4$ , which has seen significant research efforts directed towards the development of water-soluble and primarily naturally derived binders, scientific work in other cathode materials, such as  $\text{LiNi}_x\text{Mn}_{1-x-y}\text{Co}_y\text{O}_2$  (NMC), is comparatively less intensive. The main reason lies in their higher sensitivity upon contact with water, which causes the dissolution of  $\text{Li}^+$  and other transition metal ions from the material particle surface. This leads to the formation of hydroxides and carbonates, raising the slurry pH (around 10–12). Consequently, this pH elevation contributes to the corrosion of the aluminium current collector.<sup>23–25</sup> In recent times, significant attention has been directed towards NMC materials,

driven by their notable attributes of high specific capacity and average discharge voltage, which makes them very attractive for its use in electric vehicles. In this review, we have presented a thorough overview of the cutting-edge advancements in waterborne polymeric binders for the aqueous processing of high-voltage cathodes. Our focus has been specifically directed towards layered oxide NMC materials with an increasing amount of Ni in the composition.

### 1.1 Lithium-ion batteries and NMC cathode active materials

LIBs can be classified based on the atomic structure of their cathode materials, which includes layered ( $\text{LiMO}_2$ ), spinel ( $\text{LiM}_2\text{O}_4$ ), or olivine ( $\text{LiMPO}_4$ ) with M representing one or more transition metals.<sup>26</sup> One group of cathode materials that seeks to balance energy density, safety, and cost is the  $\text{LiNi}_x\text{Mn}_{1-x-y}\text{Co}_y\text{O}_2$  (NMC) family, encompassing variations such as  $\text{LiNi}_{0.33}\text{Mn}_{0.33}\text{Co}_{0.33}\text{O}_2$  (NMC 111),  $\text{LiNi}_{0.5}\text{Mn}_{0.3}\text{Co}_{0.2}\text{O}_2$  (NMC 532),  $\text{LiNi}_{0.6}\text{Mn}_{0.2}\text{Co}_{0.2}\text{O}_2$  (NMC 622) and  $\text{LiNi}_{0.8}\text{Mn}_{0.1}\text{Co}_{0.1}\text{O}_2$  (NMC 811). The relationship between thermal stability and electrochemical performance of different compositions of NMC materials is shown in Fig. 1. The distinct roles of the three transition metal ions within these materials are delineated as follows: nickel (Ni) contributes to superior capacity due to the involvement of the  $\text{Ni}^{2+}/\text{Ni}^{4+}$  couple in the deintercalation/intercalation process, enabling the extraction/insertion of 2/3 lithium ions per formula unit. However, Ni exhibits poor thermal stability. Secondly, manganese (Mn) has a lower cost than Ni and stabilizes the structure, thereby enhancing cycling performance and safety, although its capacity is lower. Finally, cobalt (Co) is responsible for boosting electronic conductivity, although it has some issues such as unethical mining practices, high cost and scarcity.<sup>28–30</sup> Particularly, nickel-rich oxides have garnered attention due to their higher reversible capacity (> than  $200 \text{ mA h g}^{-1}$ ) and specific energy ( $\sim 800 \text{ W h kg}^{-1}$ ). However, the increment of nickel content affects the reactivity

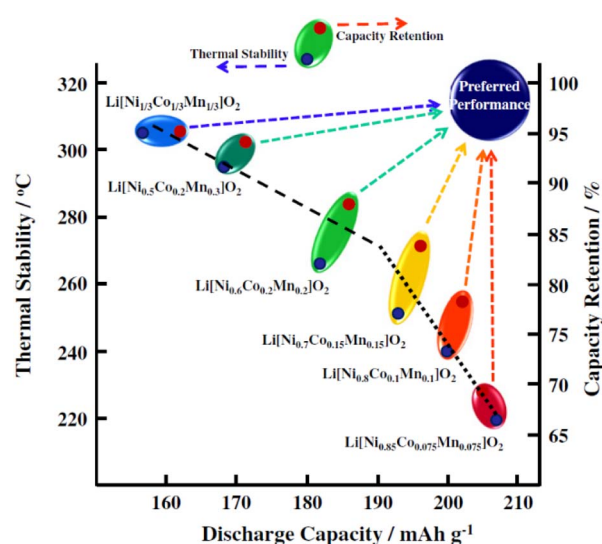


Fig. 1 Relationship between thermal stability, discharge capacity and capacity retention of different NMC materials. Reproduced with permission from ref. 27, Copyright 2013, Elsevier.



of the cathode surface with conventional carbonate-based LIB electrolytes, impacting long-term performance.<sup>13,31</sup> Furthermore, NMC materials, in general, suffer from various degradation processes, such as Li/Ni cation mixing, formation of rock salt phase (NiO), oxygen release, particle cracking, transition metal dissolution, and parasitic reactions with electrolyte.<sup>29,32</sup>

## 1.2 Functions and critical aspects of binders

In academic research, the binder content generally ranges between 3–5 wt%. Conversely, in industrial applications, in order to maximize the active material content, the binder proportion may reach 2 wt% or less. Despite the small concentration, binders play crucial functions,<sup>15</sup> and there are some key points that binders should meet for successful battery performance:

(i) Thermal stability and a broad electrochemical window to ensure prolonged battery life under harsh conditions<sup>11</sup> are particularly important for high-voltage cathode applications.<sup>33</sup>

(ii) A binder with high viscosity, which can establish repulsion forces within the particles is desired,<sup>34</sup> to provide homogeneous and well-dispersed slurries to avoid self-agglomeration of electrode components.<sup>35</sup> This property should endure over time since, in LIBs production lines, the slurries are not coated immediately, but several hours can pass before the slurry is applied.<sup>36</sup>

(iii) Effective interfacial interaction with the active particles as well as adhesion to the current collector,<sup>37</sup> by establishing strong supramolecular interactions such as ion-dipole and hydrogen bonding.<sup>38</sup> With an effective binding system, less amount of binder is required to achieve a robust adhesion, in comparison to weak van der Waals forces that tend to dissociate easily.<sup>39–41</sup> Furthermore, binders should have elasticity and flexibility to accommodate volume changes *via* deformation and relaxation and thereby avoiding the formation of cracks. Maintaining the mechanical integrity of electrodes is crucial, especially for high-loading and thick electrodes, as this is a prerequisite for implementing novel binders in the commercialization of LIBs.<sup>42–44</sup>

(iv) Exhibit good ionic and electronic conductivity to boost the diffusion of lithium ions, which is critical for the charging–discharging process.<sup>6,12</sup> Lithium ions are proposed to hop between adjacent polar moieties, such as carboxyl, hydroxyl or amino groups.<sup>15,45</sup> Therefore, the high content and uniformity of those groups contribute to the formation of a conductive network, enhancing ion transport kinetics.<sup>46</sup> The porosity of the electrode is also crucial for lithium transport and has to be optimized by applying the optimum pressure in the roll-pressing process.<sup>47–49</sup>

(v) Appropriate wetting capabilities with conventional carbonate-based electrolyte solutions, facilitating improved interaction with active materials and conductive carbon. This promotes sustained electrolyte availability during extended cycling<sup>50</sup> and creates paths for efficient conductivity and lithium-ion transport.<sup>51</sup> The solvent uptake of the binders can be enhanced by introducing a low degree of cross-linkage or polar functional groups.<sup>52</sup> However, excessive electrolyte absorption by the binder may weaken binding strength.<sup>53</sup>

(vi) The application of amorphous binders has been observed to offer more uniform covering of active material particles compared to semicrystalline polymers.<sup>54,55</sup> Effective passivation of high-voltage cathodes is required to minimize the development of microcracks caused by mechanical stress during cycling, which results in the dissolution of transition metal ions, such as Ni, Co or Mn.<sup>49,56,57</sup> Strong polar groups (such as carboxyl and hydroxyl functionalities) also improve the formation of a stable cathode electrolyte interphase (CEI) by establishing hydrogen bonding with active oxygen atoms on the surface of high-voltage cathodes.<sup>26,31,58,59</sup>

## 1.3 Conventional versus aqueous binders

Polyvinylidene fluoride (PVDF) is a commonly used polymer binder in LIBs due to its wide electrochemical window<sup>12</sup> and effective cohesion within the electrode components, and adhesion to the current collector.<sup>60</sup> However, PVDF presents a range of limitations: (i) weak van der Waals bonding system<sup>26</sup> that hampers the electrode adhesion and the interaction with the active particles of high-voltage cathodes;<sup>33,61,62</sup> (ii) its insulating nature is also an issue as it may hinder the diffusion of lithium ions;<sup>63</sup> (iii) being a fluorinated polymer, PVDF can react with lithiated graphite, forming lithium fluoride (LiF), a process that not only consumes lithium ions but also generates exothermic reactions, contributing to thermal runaway issues.<sup>30,64,65</sup> Moreover, the European Chemicals Agency (ECHA) has implemented regulations governing the utilization of per- and polyfluoroalkyl substances (PFAS) aimed at mitigating risks to human health and the environment associated with the production and application of such substances.<sup>66</sup> (iv) Use of NMP as solvent for electrode processing. The European Union regulation states that no consumer product on the market can contain more than 0.3 v/v% of NMP and that workers cannot be exposed to more than 14.4 mg m<sup>-3</sup> by inhalation and 4.8 mg kg<sup>-1</sup> per day for dermal exposure.<sup>15</sup> Therefore, the recovery of NMP as a volatile organic compound (VOC) requires significant capital investment to meet the regulations.<sup>67</sup>

Fortunately, aqueous electrode processing can achieve an environmentally friendly and cost-effective energy storage system.<sup>9</sup> Most of the aqueous binders present a large amount of hydroxyl and carboxyl functionalities which, as mentioned before, leads to better covering of the active material particles and adhesion to the current collector.<sup>15,68</sup> In terms of battery



Fig. 2 Close-loop recycling processed of aqueous processed cathodes. Reproduced with permission of ref. 16, Copyright 2022, *iScience*.



production costs, water-based electrodes consume one order of magnitude less energy during fabrication compared to NMP ones.<sup>67</sup> This efficiency is attained by accommodating a greater solid content in the slurry while maintaining coating properties. Lower drying times and temperatures are needed in the manufacturing process based on a lower boiling point, a higher vapour pressure, and a lower heat of vaporization of water.<sup>69,70</sup> Additionally, aqueous processing notably facilitates a more straightforward recycling process through the easy dissolution of the aqueous binder in water (Fig. 2),<sup>71</sup> allowing the recovery of the active materials.

#### 1.4 Challenges of the aqueous processing of NMC materials

Aqueous processing has already been achieved for graphite and silicon-based anodes, with the blend of sodium carboxymethyl cellulose (Na-CMC) and styrene butadiene rubber (SBR) as the standard binder choice.<sup>16,30,35</sup> In the case of positive electrodes, LiFePO<sub>4</sub> (LFP) is a good candidate for aqueous processing because of its low sensitivity towards water given by the strong Fe–P–O bonding.<sup>15</sup>

The main issue in the case of high-energy NMC cathode materials is the sensitivity of the active material to water.<sup>72,73</sup> As schematized in Fig. 3, protons may exchange with the lithium ions on the particle surface. As a consequence of this process, known as lithium leaching, lithium hydroxide (LiOH) and lithium carbonate (Li<sub>2</sub>CO<sub>3</sub>) are released as a sub product.<sup>74</sup>

This has two negative consequences. Firstly, the deterioration of the electrode/electrolyte interphase and in turn, the loss of electrochemically available lithium for the charge/discharge process.<sup>34,37,75</sup> To compensate for the loss of lithium, a surface reconstruction leads to the formation of a highly resistive rock salt layer (NiO) on the NMC particle and, therefore, the deterioration of the structure and particle cracking.<sup>76</sup> These issues are aggravated by the higher nickel content in the active material.<sup>77,78</sup> Additionally, the Li<sup>+</sup>/H<sup>+</sup> exchange may trigger the generation of NiOOH and nickel carbonate species (in the presence of CO<sub>2</sub>), resulting in significant cell degradation owing to the resistive nature of these compounds.<sup>79–81</sup>

The second issue is the corrosion of the current collector, which is usually aluminium in the case of cathodes. Aluminium develops an ultra-thin aluminium oxide layer (approximately 2 nm) on its surface, which acts as a robust protection from

further oxidation, stable within the pH range of 4.5 to 8.5.<sup>82</sup> However, due to the formation of LiOH and Li<sub>2</sub>CO<sub>3</sub>, the slurry alkalinity increases above pH 9, dissolves the passivating aluminium film, and corrodes the aluminium current collector.<sup>83</sup> In addition, during this process, H<sub>2</sub> gas is released, creating pores that increase the electrical resistance at the electrode/collector interphase.<sup>9,84</sup>

To address the corrosion challenge, researchers have widely adopted several strategies: (i) reduce the slurry pH through the addition of a mild acid before coating (like phosphoric acid or acetic acid)<sup>23,85–87</sup> or the use of acidic binders.<sup>88,89</sup> The use of phosphoric acid as an additive, which was firstly proposed by Passerini and coworkers for NMC 111 cathodes,<sup>87</sup> was also found to create a passivation layer on the NMC surface; (ii) decrease the pH of the aqueous slurry using a pressurized CO<sub>2</sub> gas treatment;<sup>90</sup> (iii) prevent direct contact between the aluminium surface and the corrosive slurry by applying a protective carbon coating onto the aluminium foil. This carbon coating can also improve the resistance at the interface between the cathode layer and the current collector, thereby improving electrode performance;<sup>82</sup> (iv) cover the active material particles with surface coatings composed of metal oxides (such as Al<sub>2</sub>O<sub>3</sub>, TiO<sub>x</sub> or Nb<sub>2</sub>O<sub>5</sub>)<sup>75,91–93</sup> or Li<sub>3</sub>PO<sub>4</sub><sup>36,94</sup> to prevent direct contact with water, while allowing the penetration of lithium ions through the coating during cycling.

Inferior wetting is a common issue with water-based slurries onto the aluminium current collector in comparison to NMP-based slurries, given that NMP has a lower surface tension than water. Additionally, during the evaporation of water, capillary stresses are developed, causing the deformation of particles and the propagation of cracks.<sup>95</sup>

In conclusion, the advantages and necessity of aqueous processing of cathode electrodes are clear, but there are still a few challenges to overcome, such as the corrosion of the aluminium collector, leaching of lithium ions, inferior wetting and degradation of the active material surface leading to poor electrochemical performance.

## 2 Types of aqueous binders for cathodes: considerations for binder selection in NMC electrodes

During the last few years, researchers have focused on identifying new aqueous binders for greener electrode processing,<sup>58</sup> and depending on their source, waterborne binders can be classified into two categories; synthetic or natural polymers.<sup>83</sup> Below, we cover the recent advances of waterborne binders, and their chemical structures are depicted in Fig. 4.

### 2.1 Synthetic polymers

**2.1.1 Fluorinated synthetic binders.** The most straightforward strategy to replace NMP by water is to use aqueous dispersions of conventional fluoropolymer binders, which were developed by emulsion polymerization, such as dispersions of PVDF,<sup>96,97</sup> fluoroacrylic polymer (TRD 202A)<sup>75</sup> or polytetrafluoroethylene (PTFE).<sup>37</sup> The water dispersions of those

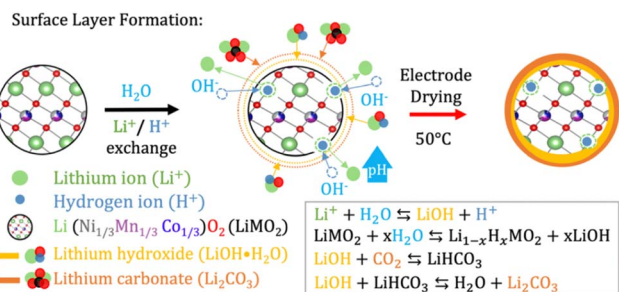


Fig. 3 Scheme of the lithium leaching degradation when nickel-rich NMC are processed *via* aqueous routes. Reproduced with permission of ref. 73, Copyright 2023, Royal Society of Chemistry.





Fig. 4 Overview of the chemical structures of natural and synthetic binders.

fluorinated binders are normally used in combination with Na-CMC, which is needed as a slurry thickener.<sup>70</sup> However, as discussed previously, fluoropolymers contain fluorine, which may be banned in the future due to toxicity, and that can also lead to thermal runaway. For these reasons, fluorine-free water-soluble synthetic binders are of interest.

### 2.1.2 Non-fluorinated synthetic binders

**2.1.2.1 Poly(acrylic acid) (PAA).** Poly(acrylic acid) (PAA) shows good mechanical stability, a long cycle life and improved lithium transport.<sup>98,99</sup> PAA is a water-soluble and high-molecular weight polymer with a large number of carboxylic acid groups ( $-\text{COOH}$ ), known to form hydrogen bonds and even ester-like chemical bonds.<sup>100,101</sup> This will result in strong supramolecular interactions, which will enhance adhesion with active material particles and with the current collector. Being an amorphous polymer, PAA can effectively stabilize the CEI. Moreover, the lithiated form of PAA, known as lithium polyacrylic acid (LiPAA), possesses the ability to supply additional  $\text{Li}^+$  ions. This capacity enables compensation for the loss of active  $\text{Li}^+$  ions during the cycling of full cells.<sup>57</sup>

**2.1.2.2 Polyacrylonitrile (PAN).** Polyacrylonitrile (PAN) is used as an aqueous emulsion and stands out as a compelling choice due to its high polarity, excellent stability, robust mechanical strength, and electrochemical stability. The nitrile groups present in PAN facilitate interactions with electroactive

and conductive materials through dipole–dipole connections, contributing to enhanced lithium conductivity.<sup>26</sup> One of the main issues with PAN is its semicrystalline nature with a high glass transition temperature ( $96.5\text{ }^\circ\text{C}$ ), resulting in rigid coatings that develop cracks during the manufacturing process.<sup>10</sup>

**2.1.2.3 Polyvinyl alcohol (PVA).** Polyvinyl alcohol (PVA) features a high number of hydroxyl groups, and as mentioned before, this property is highly sought since it leads to robust adhesive properties.<sup>26</sup> This is complemented by its dispersion properties and film-forming capabilities, which will favour a good surface coverage, crucial for mitigating transition metal dissolution.<sup>53</sup> Additionally, its wettability in common carbonate-based electrolytes ensures the uniform soaking of the electrolyte throughout the electrode, facilitating ionic mobility during cycling.<sup>51,102</sup>

**2.1.2.4 Styrene-butadiene-rubber (SBR).** Styrene-butadiene-rubber (SBR) is an elastomeric binder usually used in combination with Na-CMC. Functioning as a thickening agent, Na-CMC enhances particle dispersion, while SBR plays a pivotal role in boosting electrode flexibility and adhesion strength.<sup>103</sup>

**2.1.2.5 Poly(ionic liquid)s (PILs).** The incorporation of ionic moieties (cations and anions) into polymer structures has given rise to the family of polyelectrolytes known as poly(ionic liquid)s (PILs). PILs present fascinating strategies to enhance lithium diffusion and the mechanical integrity of the electrodes by



establishing robust bonds with the active material while retaining the structural flexibility provided by the polymer backbone.<sup>104–110</sup> For instance, pyrrolidinium PILs based on poly(diallyldimethylammonium bis(trifluoromethanesulfonyl) imide) (PDADMA-TFSI) have found applications as binders in various energy storage technologies.<sup>111–115</sup> However, those binders are not water soluble, thus, the challenges related to fluorine groups and the use of organic solvents need to be addressed for a more sustainable process. Recent literature includes water-soluble PDADMA PILs using phosphate counter anions that were applied to nickel-rich NMC 811 cathodes.<sup>116</sup>

**2.1.2.6 Conducting polymers.** An additional type of binder involves conducting polymers, and among those, the commercial poly(3,4-ethylenedioxythiophene)–polystyrene sulfonate (PEDOT:PSS) is the most widely used. This type of polymer possesses a substantial electronic conductivity ranging from 10 to  $10^2$  S cm<sup>-1</sup>. This unique characteristic allows it to serve dual purposes as both binder and conductive additive, obtaining carbon-free electrodes.<sup>114,117–119</sup> Polyethylene oxide (PEO) with high ionic conductivity and good adhesion properties has been applied as solid polymer electrolyte (SPE).<sup>120</sup>

## 2.2 Natural biopolymer binders

Nevertheless, synthetic materials such as polyacrylates, aliphatic and aromatic polymers rely on non-renewable resources such as fossil fuels. In this way, biopolymers have emerged as an exceptionally sustainable and renewable option. They are highly abundant in nature and easy to dispose of thanks to their biodegradability, coupled with their low cost and tuneability through simple functionalization.<sup>68,121</sup> Their polar units contribute to strong adhesion to the current collector and active material particles.<sup>26</sup>

**2.2.1 Sodium carboxymethyl cellulose.** Among the different biopolymers, the commercially available sodium carboxymethyl cellulose (Na-CMC) stands out among the water-soluble binders due to its outstanding properties as a binder.<sup>122,123</sup> For instance, the linear and long-chain nature of Na-CMC (Fig. 4), characterised by anionic polysaccharide properties, allows for various levels of carboxy–methyl substitution ( $-\text{OCH}_2\text{COO}^-\text{Na}^+$ ). The degree of substitution, hence the number of carboxymethyl groups per monomeric unit, plays a crucial role in its binding performance.<sup>124</sup> However, challenges such as poor mechanical properties (stiffness, brittleness and low elasticity), shrinkage due to water absorption, and low conductivity, hinder its application.<sup>10</sup> Despite these limitations, the use of Na-CMC as binder allows a higher concentration of active material by reducing the amount of binder from 5–10 wt% to 2 wt% while maintaining performance.<sup>68</sup> This has motivated researchers to explore alternative biopolymers as potential binders.

**2.2.2. Sodium Alginate** Derived from brown algae, sodium alginate (SA) stands out for its robust bonding system, attributed to the presence of carboxylic groups along the polymer backbone that enhance interactions with the active material and increase adhesion strength.<sup>62</sup> Moreover, the introduction of metal cations is a strategy for transition metal ion chelation through the formation of an egg-box structure.<sup>125</sup> Such

structures minimise the metal leaching from the active materials into the electrolyte.

**2.2.3 Carboxymethyl chitosan.** Another interesting biopolymer is carboxymethyl chitosan (C-CTS) obtained by carboxymethylation of chitosan, which presents large-scale availability. The presence of amino and hydroxyl functions imparts a unique status to this sustainable biopolymer as a cross-linkable polymer that can effectively interconnect with active materials through hydrogen bonding.<sup>126</sup> Moreover, the robust electron-donating characteristics of the amine group contribute to the enhancement of electronic conductivity.<sup>127</sup>

**2.2.4 Gums.** Gums such as guar gum (GG) and xanthan gum (XG) are soluble in water and commonly used in the food industry. Gums are attractive options owing to their robust structures featuring multiple polar groups. These attributes contribute to favourable rheological behaviour, mechanical stability, effective coordination with transition metals, and facilitation of lithium-ion diffusion within the electrode.<sup>128–130</sup>

**2.2.5. Carrageenan.** Finally, another interesting family of water-soluble binders is based on carrageenan biopolymers, which are linear sulfonated polymers with one, two or three sulfonate ( $\text{SO}_3^-$ ) groups, known as kappa, iota and lambda carrageenan, respectively.<sup>131</sup> Carrageenan is considered an interesting option as a binder due to its high viscosity, natural availability, low cost, and molecular interactions given by the presence of sulfonate groups that can also enhance lithium diffusion.<sup>132–134</sup>

## 3 Performance of aqueous binders in NMC electrodes: electrochemical performance, rate capability, cycling stability and capacity retention, effects on NMC particle degradation

In recent times, the aqueous processing of  $\text{LiNi}_{0.33}\text{Mn}_{0.33}\text{Co}_{0.33}\text{O}_2$  (NMC 111) has garnered more attention due to its relative low water sensitivity in comparison with higher nickel content structures. Conversely, there has been a recent exploration of high nickel-content materials like  $\text{LiNi}_{0.6}\text{Mn}_{0.2}\text{Co}_{0.2}\text{O}_2$  (NMC 622) and  $\text{LiNi}_{0.8}\text{Mn}_{0.1}\text{Co}_{0.1}\text{O}_2$  (NMC 811) for aqueous processing. This review primarily focuses on the recent developments, summarising their main processing parameters (formulation wt% and loading) and outcomes (cell configuration and electrochemical performance) in Table 1.

### 3.1 NMC 111

In the realm of aqueous processing of NMC 111, thorough investigations have been conducted employing various materials such as Na-CMC,<sup>82,87,135,163–166</sup> guar gum,<sup>167</sup> polyurethane<sup>168</sup> and poly acrylic acid.<sup>120,169,170</sup> The focal points of these studies were to improve the mechanical properties of NMC 111 cathodes and to mitigate aluminium collector corrosion. The details of these reports will not be extensively explored here, as they have already been comprehensively discussed in various reviews.<sup>8,10,13,15,26,28,30,83,171</sup>



Table 1 Summarized parameters of different reports of aqueous processing of NMC materials

Composition	Binder	Cell, anode and electrolyte	Loading – porosity/density	Voltage	Discharge (mA h g <sup>-1</sup> )	Capacity retention	Comments	Ref.
<b>LiNi<sub>0.33</sub>Mn<sub>0.33</sub>Co<sub>0.33</sub>O<sub>2</sub> (NMC 111)</b>								
88 wt% NMC	Na-CMC	Pouch cells	7.64 mg cm <sup>-2</sup>	2.75–4.2 V	124 (1C)	84% (1000 cy. 1C)	CC-Al optimized	135
7 wt% C <sub>45</sub>		Graphite anode	1.88 g cm <sup>-3</sup> density	CCCV		70% (2000 cy. 1C)	calendaring force 70 kg cm <sup>-1</sup>	
5 wt% Na-CMC		1 M LiPF <sub>6</sub> EC : DMC 1 : 1 w/w						
		Polyethylene separator						
88 wt% NMC	Na-CMC	Pouch cells	8.2 mg cm <sup>-2</sup>	3.0–4.2 V	127 (1C)	96% (311 cy. 1C)	1 wt% of PA	87
7 wt% C <sub>45</sub>		Graphite anode	calendared 70 kg cm <sup>-1</sup>	CCCV				
5 wt% Na-CMC		1 M LiPF <sub>6</sub> EC : DMC 1 : 1 w/w + 1 wt% VC						
		PE separator						
90 wt% NMC	Lignin	Coin cells	7.4 ± 0.3 mg cm <sup>-2</sup>	3.0–4.3 V	154 (0.1C)	89% (100 cy. 0.5C)	CC-Al wetting of 35 days before cycling	73
5 wt% C <sub>45</sub>		Lithium anode	cm <sup>-2</sup> 45–50% porosity	CCCV				
5 wt% lignin		1 M LiPF <sub>6</sub> in EC : DMC : DEC 1 : 1 : 1						
		Celgard 2320						
<b>LiNi<sub>0.4</sub>Mn<sub>0.4</sub>Co<sub>0.2</sub>O<sub>2</sub> (NMC 442)</b>								
80 wt% NMC	Na-CMC	Coin cells	2 mg cm <sup>-2</sup>	3.0–4.3 V	161 (0.1C)	99% (100 cy. 1C)	One drop of PA	122
15 wt% C <sub>45</sub>		Lithium anodes	calendared 9 ton per cm <sup>2</sup>					
5 wt% Na-CMC		1 M LiPF <sub>6</sub> in EC : DMC 1 : 1 v/v + 2% VC						
		Polyethylene separator						
<b>LiNi<sub>0.5</sub>Mn<sub>0.3</sub>Co<sub>0.2</sub>O<sub>2</sub> (NMC 532)</b>								
85 wt% NMC	PUGLY (pullulan: glycerol 1 : 1)	Swagelok cells	5.6 mg cm <sup>-2</sup>	2.5–4.2 V	115 (0.1C)	—	Al foil immersed in 5 wt% KOH to remove passivation layer	17
10 wt% C <sub>45</sub>		Lithium anodes	calendared 4 ton per cm <sup>2</sup>					
5 wt% PUGLY		1 M LiPF <sub>6</sub> in EC : DMC 1 : 1 w/w						
		Celgard 2300						
96.2 wt% NMC	30% Li-CMC + 70% polyacrylic acid/acrylate copolymer	Cylindrical 18 650 cell	2000 mA h	3.0–4.2 V	161 (0.2C)	89% (1200 cy. 1C)	0.3 wt% boric acid as pH modifier	136
2 wt% carbon		Graphite anodes		CCCV				
0.8 wt% CNT		Polyethylene separator						
1.5 wt% binder	Na-CMC-PEO	Pouch cell	15–18 mg cm <sup>-2</sup>	2.8–4.15 V	850 mA h (0.1C)	89% (1000 cy. 1C)		137
93 wt% NMC		Graphite	calendared 10% thick. Red					
4 wt% SuperP		1 M LiPF <sub>6</sub> EC : DMC : DEC 1 : 1 : 1						
2 wt% PEO		Pouch cell	25 mg cm <sup>-2</sup>	2.5–4.2 V		97% (95 cy. 0.33C)	20 wt% of IPA as cosolvent	95
1 wt% Na-CMC	Na-CMC + acrylic emulsion	Graphite anodes						
90 wt% NMC		1.2 M LiPF <sub>6</sub> EC : DMC 3 : 7 w/w						
5 wt% carbon		Celgard 2325						
1 wt% Na-CMC								
4 wt% emulsion								





Table 1 (Contd.)

Composition	Binder	Cell, anode and electrolyte	Loading – porosity/density	Voltage	Discharge (mA h g <sup>-1</sup> )	Capacity retention	Comments	Ref.
90 wt% NMC 5 wt% carbon 1 wt% Na-CMC	Na-CMC + PVDF latex	Pouch cell Graphite anodes 1.2 LiPF <sub>6</sub> in EC : DEC 3 : 7 w/w	1200 mA h 50% porosity	2.5–4.2 V	—	80% (864 cy. 0.33C)	Corona plasma of Al to enhance wetting	16
4 wt% latex 90.5 wt% NMC 4 wt% C <sub>65</sub> 1.5 wt% CMF	Na-CMC + PEO + PAA	Celgard 2325 Coin cells Graphite anodes 1 M LiPF <sub>6</sub> in EC : DMC 3 : 7 w/w	2 mA h cm <sup>-2</sup> 40% porosity	3.0–4.2 V CCCV	135 (1C)	81 (500 cy. 1C)	CC-Al LiOH for pH 12.5	138
1 wt% Na-CMC 1 wt% PEO 1 wt% PAA 91.5 wt% NMC 4 wt% C <sub>65</sub> 1.5 wt% CMF	Na-CMC + PEO + PAA	Coin cells	2 mA h cm <sup>-2</sup> 40% porosity	3.0–4.2 V CCCV	—	85 (500 cy. 1C)	CC-Al LiOH for pH 12.5 CTAB surfactant	139
1 wt% Na-CMC 1 wt% PEO 1 wt% PAA 92 wt% NMC 4 wt% C <sub>65</sub> 1 wt% Na-CMC	Na-CMC + latex binder	Graphite anodes, CC-Al, polyolefin, 1LiPF <sub>6</sub> EC : EMC Coin cells Graphite anodes 1 M LiPF <sub>6</sub> in EC : PC : DMC 1 : 1 : 3 weight + 2% VC	11.5 mg cm <sup>-2</sup> 35% porosity	2.5–4.2 V	154 (0.1C)	—	1 wt% NMC of PA as pH modifier	86
3 wt% latex 94.5 wt% NMC 2 wt% C <sub>65</sub> 1 wt% Na-CMC	Na-CMC + latex binder	Celgard 2400 Coin cells Lithium anodes 1 M LiPF <sub>6</sub> in EC : PC : DMC 1 : 1 : 3 weight	11.5 mg cm <sup>-2</sup> 30% porosity	3.0–4.3 V CCCV	—	94% (200 cy. 1C)	0.5 wt% <sub>total solids</sub> of PA as pH modifier	140
2 wt% latex 0.5 wt% PA		Celgard 2400						
<b>LiNi<sub>0.6</sub>Mn<sub>0.2</sub>Co<sub>0.2</sub>O<sub>2</sub> (NMC 622)</b> 92 wt% NMC 3 wt% C <sub>45</sub> 2 wt% Na-CMC	Na-CMC + PVDF latex	Coin cells Graphite anodes 1 M LiPF <sub>6</sub> in EC : DMC 1 : 1 + 2% VC	3 mA h cm <sup>-2</sup> 35% porosity	2.8–4.3 V	143 (1C)	80% SOH (265 cy. 1C)	CC-Al 1 wt% NMC of PA	141
3 wt% latex 92 wt% NMC 5 wt% C <sub>65</sub> 3 wt% Na-CMC	Na-CMC	Celgard 2500 Coin cells Lithium anodes 1 M LiPF <sub>6</sub> EC : DMC 1 : 1	6 mg cm <sup>-2</sup> calendared	3.0–4.3 V CCCV	159 (0.1C) 137 (1C)	78% (396 cy. 1C)	0.5 wt% NMC of PA electrodes washed with ethanol	142
100 wt% NMC 2 wt% C <sub>65</sub> 2 wt% Na-CMC 3 wt% TRD202A	Na-CMC + TRD202A	Celgard 2400 Coin cells Lithium foil 1.3 M LiPF <sub>6</sub> EC/DMC 3 : 7 + 5 wt% FEC	34–47 mg cm <sup>-2</sup> 35% porosity	3.0–4.3 V CCCV	70 (1C)	—	Acetic acid pH 10 structured electrodes with laser patterning	143

Table 1 (Contd.)

Composition	Binder	Cell, anode and electrolyte	Loading – porosity/density	Voltage	Discharge (mA h g <sup>-1</sup> )	Capacity retention	Comments	Ref.
92.6 wt% NMC 2.8 wt% C <sub>65</sub> 0.8 wt% Na-CMC	Na-CMC + TRD202A	Coin cells Lithium foil 1.3 M LiPF <sub>6</sub> EC/DMC 3 : 7 + 5 wt% FEC Celgard 2500	35 mg cm <sup>-2</sup> 35% porosity	3.0–4.3 V CCCV	125 (0.5C)	72% (80 cy. 0.5C)	Acetic acid pH 10 structured electrodes with laser patterning	144
2.8 wt% TRD202A 89.5 wt% NMC 5 wt% carbon 1 wt% Na-CMC 4 wt% TRD202A	Na-CMC + TRD202A	Coin cells Graphite anodes 1.2 M LiPF <sub>6</sub> in EC : EMC 3 : 7 w/w	2 mA h cm <sup>-2</sup> / 11.12 mg cm <sup>-2</sup>	3.0–4.3 V		120 mA h g <sup>-1</sup> after 350 cy. 1C	0.5 wt% PA, coating with SiO <sub>2</sub>	145
<b>Li<sub>0.8</sub>Mn<sub>0.1</sub>Co<sub>0.1</sub>O<sub>2</sub> (NMC 811)</b> 90 wt% NMC 5 wt% carbon 1 wt% Na-CMC	Na-CMC + acrylic emulsion	Single layer pouch cells Lithium anodes 1.2 M LiPF <sub>6</sub> in EC : EMC 3 : 7 w/w	11.3–11.6 mg cm <sup>-2</sup> 35% porosity	2.5–4.2 V CCCV	198 (0.1C) 136 (3C)	70% (1000 cy. 0.33C)	Corona treatment for aluminium foil	78
4 wt% emulsion 94 wt% NMC 3 wt% carbon 3 wt% PAA	PAA	Celgard 2325 Coin cells Lithium anodes 1.15 M LiPF <sub>6</sub> in EC : DEC : EMC 3 : 3 : 4 v/v + 5 wt% FEC	Calenderer 7.5 ton per cm <sup>-2</sup>	3.0–4.3 V	198 (0.1C) 189.2 (0.2C) 160 (2C)	84.2 (100 cy. 0.2C)		88
94 wt% NMC 3 wt% carbon 3 wt% PAA	PAA	Celgard 2500 Coin cells Lithium anodes 1.15 M LiPF <sub>6</sub> in EC : DEC : EMC 3 : 3 : 4 v/v + 5 wt% FEC	16–18 mg cm <sup>-2</sup> calendared 7.5 ton per cm <sup>2</sup>	3.0–4.3 V	180 (0.2C cycle 1) 188 (0.2C cycle 5)	96% (100 cy. 0.2C compared to cycle 5)	NMC powder modified with PA	146
90 wt% NMC 5 wt% carbon 1 wt% Na-CMC	Na-CMC + TRD202A	Celgard 2500 Pouch cells Graphite anodes 1.3 M LiPF <sub>6</sub> in EC : EMC 3 : 7 w/w	6–8 mA h cm <sup>-2</sup> 30% porosity	3.0–4.2 V	190 (0.1C)	—	1 wt% of PA	147
4 wt% TRD202A 90 wt% NMC 7 wt% C <sub>65</sub> 3 wt% Na-CMC	Na-CMC	Celgard 2325 Pouch cell Lithium anodes 1 M LiPF <sub>6</sub> EC : DMC 1 : 1 w/w	12 ± 2 mg cm <sup>-2</sup> 50% reduction porosity	2.0–4.3 V CCCV	188.8 (0.1C)	92% (20 cy. 1C)		148
99.47 wt% NMC 0.15 wt% SWCNT 0.25 wt% locust bean gum 0.13 wt% xanthan gum	Locust bean + xanthan gum	Celgard 2500 Coin cells Lithium anodes 1 M LiPF <sub>6</sub> EC : DMC : EMC 1 : 1 : 1 v/v	511 mg cm <sup>-2</sup> 40% porosity	2.8–4.3 V	155 (0.05C)	79% (10 cy. 0.05C)	Freeze drying	149





Table 1 (Contd.)

Composition	Binder	Cell, anode and electrolyte	Loading – porosity/density	Voltage	Discharge (mA h g <sup>-1</sup> )	Capacity retention	Comments	Ref.
86.1 wt% NMC 9.6 wt% carbon 4.3 wt% PAN	PAN	Coin cells Lithium anodes 1.15 M LiPF <sub>6</sub> in EC: DEC : EMC 3 : 3 : 4 + 5 wt% FEC	—	3.0–4.3 V	150 (0.5C)	100% (100 cy. 0.5C)	Carbon fabric current collector	150
92 wt% NMC 3 wt% C <sub>65</sub> 2 wt% Na-CMC	Na-CMC + poly(meth)acrylate (PMA)	Coin cells Graphite anodes 1M LiPF <sub>6</sub> 3 : 7 EC : DMC + 2 wt% VC	8.6 mA h cm <sup>-2</sup> 40% porosity	3.0–4.2 V CCCV	171 (0.2C) 136 (0.5C) 65 (1C)	—	0.16 g of PA per g of NMC 811 double layer technique	151
1 wt% PMA 92 wt% NMC 3 wt% C <sub>65</sub> 2 wt%	Na-CMC + poly(meth)acrylate (PMA)	Coin cells Graphite anodes 1 M LiPF <sub>6</sub> 3 : 7 EC : DMC + 2 wt% VC	8.6 mA h cm <sup>-2</sup> 40% porosity	3.0–4.2 V CCCV	173 (0.1C) 158 (0.2C) 156 (0.5C)	91% (100 cy. 1C)	0.16 g PA for g NMC binder reduction of PMA on top layer from 2 wt% to 0.5 wt%	152
Graphite 1 wt% Na-CMC 2 wt% PMA		Celgard 2500			82 (1C)			
90 wt% NMC 5 wt% carbon 1 wt% Na-CMC	Na-CMC + JSR (fluorine acrylic hybrid latex)	Single layer pouch cells Graphite anodes 1.2 M LiPF <sub>6</sub> in EC : EMC 3 : 7 w/w	9.8 mg cm <sup>-2</sup> 35% porosity	2.5–4.2 V CCCV	195 (0.1C) 187 (0.33C) 136 (3C)	60% (1000 cy. 0.33C)	Corona treatment for aluminium foil	70
4 wt% latex 94 wt% NMC 3 wt% C <sub>65</sub> 3 wt% PAA	PAA	Coin cells Graphite anodes 1 M LiPF <sub>6</sub> in 1 : 1 EC : EMC w/w	2.1 mA h cm <sup>-2</sup> calendared	3.0–4.3V	172 (0.2C)	95% (100 cy. 0.2C)		153
91 wt% NMC 5 wt% C <sub>45</sub> 1 wt% Na-CMC 3 wt% TRD202A	Na-CMC + TRD202A	Glass fibre separator Pouch cells Lithium anode 1 M LiPF <sub>6</sub> in EC : DMC 1 : 1 v/v Whatman glass fibre separator	3.2 ± 0.2 mg cm <sup>-2</sup> calendared	3.0–4.3 V	201 (0.1C) 128 (5C) 84 (10C)	Similar to PVDF after 100 cy. 0.33C for 100 cycles	1 wt% <sub>total solids</sub> of PA	154
92 wt% NMC 3 wt% C <sub>65</sub> 1.5 wt% Na-CMC	Na-CMC + acrylate binder	Coin cells Graphite anodes 1 M LiPF <sub>6</sub> in EC : EMC 3 : 7 v/v	12 mg cm <sup>-2</sup> porosity	2.8–4.2 V CCCV	191 (0.1C) 173 (1C)	86% (400 cy. 1C)	CC-Al <sub>2</sub> 2 wt% <sub>total solids</sub> of lithium sulphate	155
1.5 wt% acrylate binder 2 wt% lithium sulphate 70 wt% NMC 20 wt% acetylene black	Poly-1-vinyl-2-pyrrolidone-	Coin cells Lithium anodes	7.4 mg cm <sup>-2</sup>	3.0–4.3 V	233 (0.1C) 215 (0.2C)	96% (100 cy. 0.1C) 94% (200 cy. 1C)		156

Table 1 (Contd.)

Composition	Binder	Cell, anode and electrolyte	Loading – porosity/density	Voltage	Discharge (mA h g <sup>-1</sup> )	Capacity retention	Comments	Ref.
10 wt% binder	crosslinked-prop-2-enoic acid (poly(VPCPEA))	1.1 M LiPF <sub>6</sub> in DMC; EMC 1 : 1 v/v			209 (0.3)			
90 wt% NMC	Poly(diallyl dimethylammonium diethyl phosphate) (PDADMA-DEP)	Coin cells	12 mg cm <sup>-2</sup> 40% porosity	2.8–4.3 V	191 (0.5C) 156 (1C) 200 (0.1C) 101 (5C)	91 (90 cy. 0.5C)	CC-Al	116
5 wt% C <sub>45</sub>		Graphite anodes						
5 wt% binder		1 M LiPF <sub>6</sub> ED; DMC 1 : 1 + 2% VC						
93 wt% NMC	3 SO <sub>3</sub> -carrageenan	Glass fibre separator	12 mg cm <sup>-2</sup> 40% porosity	2.8–4.3 V	200 (0.1C) 133 (3C) 105 (5C)	91 (90 cy. 0.5C)	CC-Al	134
5 wt% C <sub>45</sub>		Coin cells						
2 wt% binder		Graphite anodes						
		1 M LiPF <sub>6</sub> ED; DMC 1 : 1 + 2% VC						
90 wt% NMC	Na-CMC + biobased latex	Glass fibre separator	12 mg cm <sup>-2</sup> 40% porosity	2.8–4.3 V	128 (3C) 100 (5C)	84 (90 cy. 0.5C)	CC-Al	157
5 wt% C <sub>45</sub>		Coin cells						
2 wt% Na-CMC		Graphite anodes						
		1 M LiPF <sub>6</sub> ED; DMC 1 : 1 + 2% VC						
3 wt% biobased latex		Glass fibre separator						
85 wt% NMC	Na-CMC + SBR	Coin cells		2.8–4.3 V	189 (0.1C) 94 (10C)	99.9% (100 cy. 0.5C)	CC-Al 0.5% <sub>NMC</sub> of acetic acid dispersing agent	158
10 wt% carbon		Lithium anode					water: Ethanol 9 : 1	
2 wt% Na-CMC		1 M LiPF <sub>6</sub> in EC; DEC 1 : 1 v/v						
3 wt% SBR		Microfiber glass separator						
92 wt% NMC	Na-CMC	Pouch cells	2 mA h cm <sup>-2</sup> 50% porosity	2.7–4.2 V	150 (0.5C)	94% (450 cy. 0.5C)	Phosphate-coated NMC 811 particles by spray drying	159
4 wt% C <sub>65</sub>		Graphite anodes		CCCV				
4 wt% Na-CMC		1 M LiPF <sub>6</sub> in EC; EMC 3 : 7 + 2 wt% VC						
		Celgard 2325						
92 wt% NMC	Na-CMC + SBR + PAA	Coin cells	20.5 mg cm <sup>-2</sup> 3.1 g cm <sup>-3</sup>	3.0–4.3 V	199 (0.1C) 180 (0.5C)	—	0.16 mmol PA per g of NMC 811 water: isopropanol 80 : 20 wt%	59
5 wt% C <sub>45</sub>		Lithium anodes		CCCV				
1 wt% Na-CMC		1 M LiPF <sub>6</sub> in EC; EMC 3 : 7 vol% + 2 wt% VC						
1 wt% SBR		Glass fibre separator						
1 wt% PAA								
80 wt% NMC	DSS-co-LiPAA	Coin cells	4.5–4.7 mg cm <sup>-2</sup>	2.8–4.3 V	206 (100 mA g <sup>-1</sup> )	89.4% (200 cy. 100 mA g <sup>-1</sup> )		160
10 wt% Super P		Lithium anodes						
10 wt% DSS-co-LiPAA		1 M LiPF <sub>6</sub> in DC; EC; EMC 1 : 1 : 1 vol% + phenyl sulfoxide						
		Polypropylene separator						





Table 1 (Contd.)

Composition	Binder	Cell, anode and electrolyte	Loading – porosity/density	Voltage	Discharge (mA h g <sup>-1</sup> )	Capacity retention	Comments	Ref.
<b>LiNi<sub>0.83</sub>Mn<sub>0.05</sub>Co<sub>0.12</sub>O<sub>2</sub></b>								
94.4 wt% NMC	Na-CMC + SBR	Bilayer pouch cell	14.3 mg cm <sup>-2</sup>	2.7–4.2 V	195 (0.1C)	83.6% (1000 cy. 1C)	0.5 wt% <sub>NMC</sub> of PA	161
3 wt% C <sub>65</sub>		Graphite anodes	2.6 mA h cm <sup>-2</sup>	CCCV	177 (1C)			
1 wt% graphite		1.4 M LiPF <sub>6</sub> in EC : DMC 3 : 7 w/w + 2% VC Celgard H1609	3.5 g cm <sup>-3</sup>					
0.6 wt% Na-CMC								
1 wt% SBR	Na-CMC + SBR	Bilayer pouch cell	3.0–3.1 mA h cm <sup>-2</sup>	2.7–4.2 V	201 (0.1C)	79.3% (1000 cy. 1C)	CC-Al 0.5 wt% <sub>NMC</sub> of PA 5 kg slurries	162
94 wt% NMC				CCCV				
3 wt% C <sub>65</sub>		Graphite anodes	3.2 mg cm <sup>-3</sup>		100 (5C)	75% (2000 cycles 1C)		
1 wt% graphite		1.4 M LiPF <sub>6</sub> in EC : DMC 3 : 7 w/w + 2% VC Celgard H1609						
1 wt% Na-CMC								
1 wt% SBR	Na-CMC + SBR	Bilayer pouch cell	3.0–3.1 mA h cm <sup>-2</sup>	2.7–4.2 V	188 (1C)	80% (1700 cy. 1C)	CC-Al 0.5 wt% <sub>NMC</sub> of PA lower temperature of 2nd drying to 80 °C (instead of 140 °C)	76
94 wt% NMC				CCCV				
3 wt% C <sub>65</sub>		Graphite anodes	3.2 mg cm <sup>-3</sup>					
1 wt% graphite		1.4 M LiPF <sub>6</sub> in EC : DMC 3 : 7 w/w + 2% VC Celgard H1609						
1 wt% Na-CMC								
1 wt% SBR	Na-CMC + ICN	Bilayer pouch cell	14.3 mg cm <sup>-2</sup>	2.7–4.2 V	182 (0.1C)	88% (1000 cy. 1C)	0.5 wt% <sub>NMC</sub> of PA	72
93 wt% NMC				CCCV				
3 wt% C <sub>65</sub>	(polyisocyanate-based binder)	Graphite anodes	2.6 mA h cm <sup>-2</sup>					
1 wt% graphite		1.4 M LiPF <sub>6</sub> in EC : DMC 3 : 7 w/w + 2% VC Celgard H1609	3.5 g cm <sup>-3</sup>					
2 wt% Na-CMC								
1 wt% ICN								

In recent investigations, the application of kraft lignin as a binder for water processed NMC 111 cathodes has been explored. Rheological assessments have revealed that replacing the traditional NMP solvent with water permits a decrease in solvent amount to attain equivalent slurry viscosity. To address surface cracks and mitigate binder migration, reducing the temperature in the drying process to 50 °C was implemented. The incorporation of lignin as a binder has shown robust cohesive forces within the electrode, particularly between carbon black (CB) and NMC 111 particles. Additionally, the mechanical strength of the coating has been enhanced by carbon-coated aluminium foil. Unfortunately, the lignin-based cathodes demonstrated inferior electrolyte wetting. Nevertheless, when extending the electrolyte soaking time before cycling, lignin-based NMC 111 cells exhibited promising performance, delivering 154 mA h g<sup>-1</sup> at 0.5C and maintaining 89% capacity retention after 100 cycles. This performance was comparable to that of PVDF-based cathodes (153 mA h g<sup>-1</sup> and 93%).<sup>73</sup> Lignin-based cathodes with improved ionic and electrical conductivity have been fabricated using laser structuring of calendared electrodes (thickness ~150 μm).<sup>172</sup>

### 3.2 NMC 532

The utilisation of mild acids to modulate the pH of NMC slurries and avoid aluminium collector corrosion has been proposed in several studies. However, the impact of these mild acids on the performance of the active material remains a topic of ongoing debate. In their study, Bichon *et al.* observed increased lithium extraction when phosphoric acid (PA) was present in the aqueous processing of NMC 532 electrodes. Notably, in the presence of phosphoric acid, transition metal and lithium phosphates are formed instead of LiOH and Li<sub>2</sub>CO<sub>3</sub>, which help to stabilise the cathode electrolyte interface (CEI) and improve lithium diffusion by the formation of the good ionic conductor Li<sub>3</sub>PO<sub>4</sub>.<sup>140</sup> The PA-NMC 532 aqueous cathode exhibited cycling stability comparable to that of the PVDF cell. However, there was an initial capacity reduction attributed to lithium loss and increased polarisation.<sup>86</sup>

Ibing *et al.*<sup>138</sup> investigated more in detail the influence of binder pH on the performance of NMC 532 electrodes, using as binder a composition of 1 : 1 : 1 wt% of polyacrylic acid (PAA), polyethylene oxide (PEO), and carboxymethyl cellulose (Na-CMC) and a carbon-coated aluminium current collector. The synergistic use of binders can improve the mechanical properties of the electrodes, due to a combination of their elastic characteristics or through crosslinking interactions between them (*e.g.* Na-CMC with PAA).<sup>59</sup> Considering the Li<sup>+</sup> and proton equilibrium reaction (1) on the NMC surface:



It becomes evident that employing a low pH slurry with a high proton concentration would favour the shift towards H-NMC. In response to this, the authors introduced an alternative additive, lithium hydroxide (LiOH), which was used to regulate the pH of the binder solution (prior to adding active and conductive materials) and explored two distinct scenarios with

pH values of 7.6 and 12.5. After 500 cycles at 1C, a state of health (SOH) of 81% was reached for cells with a starting pH of 12.5, while organic PVDF electrodes demonstrated an 88% SOH. Conversely, a pH value of 7.6 resulted in a more pronounced fading, with a SOH of 68% under identical conditions. This decline in performance was attributed to an increased lithium-proton exchange. In this case, the lithium extracted from the NMC material during cycling reacted with the electrolyte, forming surface species such as Li<sub>2</sub>CO<sub>3</sub> and LiOH. The subsequent formation of water could lead to the decomposition of the LiPF<sub>6</sub> salt, ultimately resulting in the formation of LiF.<sup>138</sup>

Using this composition for NMC 532 electrodes and adding LiOH for an optimised pH of 12.5 for the starting binder solution, the authors also explored the use of hexyldecyltrimethylammonium bromide (CTAB) as a surfactant to improve the dispersibility and distribution of particles, as well as the carbon black coverage of the active material. Upon employing 0.3 wt%<sub>NMC 532</sub> of surfactant, a marked improvement in rate capability was observed in contrast to conventional PVDF (119 vs. 83 mA h g<sup>-1</sup> at 5C, respectively). Nevertheless, an increase in the surfactant concentration to 0.5 wt%<sub>NMC 532</sub> resulted in a deterioration, attributed to free CTAB within the electrode, which contributed to an increase in cell impedance. Notably, extended cycling of the aqueous NMC 532 electrodes with 0.3%<sub>NMC 532</sub> revealed a slight decrease in specific discharge capacities over time. Nevertheless, the capacity retentions remained comparable to PVDF/NMP-based references after 500 cycles at 1C (85% and 87%, respectively).<sup>139</sup>

Areal loading is a critical factor in commercial batteries to obtain a balance between cost and performance. Unfortunately, increasing the loading of aqueous NMC 532 electrodes from 15 to 25 mg cm<sup>-2</sup> results in cracks across the electrode surface, which cannot be solved by conventional calendaring methods. The root cause lies in the capillary pressure generated during drying. To address this issue, the incorporation of isopropyl alcohol (IPA) as a co-solvent was proposed by Du *et al.* to reduce surface tension in comparison to water. Notably, the 80/20 wt% (water/IPA) ratio demonstrated optimal performance, allowing crack-free electrodes and exhibiting a capacity retention of 97.3% after 95 cycles at 0.33C, comparable to the 97% achieved with polyvinylidene fluoride (PVDF).<sup>95</sup>

Another solution to tackle crack formation was to employ multiple layers of coating, layered one upon the other, which successfully preserved electrochemical performance without exhibiting cracks in optical images. As expected, when increasing the thickness of NMC 532 electrodes using as binder Na-CMC and styrene butadiene rubber (SBR) in a 1 : 2 ratio, a performance decline was observed due to a kinetic impediment where lithium-ion diffusion became hindered. Intriguingly, the substitution of SBR with polyethylene oxide (PEO) mitigated the cracking issue, demonstrating a crack-free monolayer coating even at elevated loadings. The high molecular weight and polar structures of PEO facilitated the formation of robust and stable bonds, capable of maintaining the structural integrity of the electrodes. Pouch cells incorporating NMC 532 cathodes with a Na-CMC/PEO binder system, loaded at 15.8 mg cm<sup>-2</sup>, and graphite anodes exhibited an impressive





Fig. 5 Recycling of water-based electrodes using pullulan as binder by water spraying. Reproduced with permission of ref. 17, Copyright 2022, Elsevier.

capacity retention of 89% at a 1C rate after 1000 cycles. This performance was comparable to that of PVDF-cells, which achieved 90% retention under identical conditions, albeit using toxic NMP instead of water as the solvent.<sup>137</sup>

Cui *et al.* employed a combination of lithium carboxymethyl cellulose (Li-CMC) and a commercial polyacrylic latex copolymer (306F) to enhance lithium conduction and improve the mechanical strength in the aqueous processing of cylindrical batteries with a nominal capacity of 2000 mA h. To address the challenge of aluminium collector corrosion, the authors used boric acid to maintain the slurry pH within the range of 9.0–10.0. This hybrid Li-CMC-306F binder exhibited superior adhesion properties attributed to the formation of hydrogen bonds, resulting in an impressive capacity retention of 88.9% after 1200 cycles at 1C, compared to 80.6% for organic PVDF-cell under identical conditions.<sup>136</sup>

Pullulan, another water-soluble and biodegradable polymer employed in the production of NMC 532 cathodes, emerges as a promising binder with a remarkable 70% cost reduction compared to PVDF–NMP. Furthermore, NMC 532 processed with water using pullulan as a binder demonstrated performance comparable to traditional PVDF electrodes. At 0.1C, both cells delivered 115 mA h g<sup>-1</sup>, and at 1C, PVDF–NMC 532 showed 99 mA h g<sup>-1</sup>, while pullulan–NMC 532 exhibited 96 mA h g<sup>-1</sup>. The water-based process not only facilitates the environmentally friendly recovery of NMC and carbon black powders but also ensures a method that is cost-effective and rapid (Fig. 5). The recycled powders can be efficiently collected using biodegradable wastewater. Under aerobic conditions, the pullulan solution achieved 34% biodegradability within 15 days, showcasing its eco-friendly contribution to the sustainability of the manufacturing process in contrast to PVDF.<sup>17</sup>

### 3.3 NMC 622

To substantiate the viability of aqueous cathode processing, a scaling-up involving NMC 622 slurries with a total solid content of 500 g was reported, employing Na-CMC and PVDF latex as binders. Unfortunately, the electrodes exhibited cracking at high loadings (3 mA h cm<sup>-2</sup>) and although changes

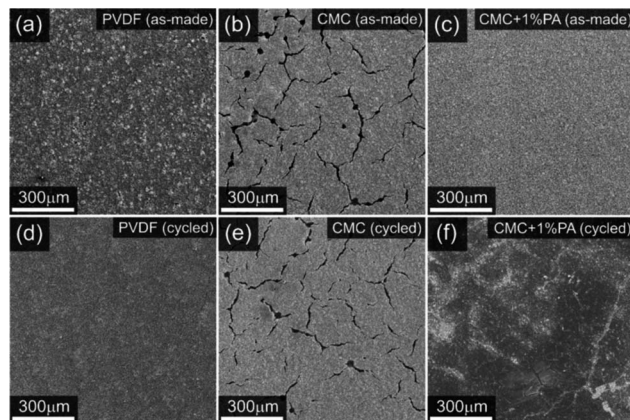


Fig. 6 Secondary electron images of electrodes before and after cycling with different binders. (a) and (d) PVDF, (b) and (e) CMC and (c) and (f) CMC + 1% of phosphoric acid (PA). Reprinted with permission of ref. 142, Copyright 2023, RSC.

in temperature and convective flux showed some improvements, the addition of 1 wt% PA<sub>NMC 622</sub> phosphoric acid was necessary to mitigate the cracks. Nevertheless, for industrial manufacturing, carbon-coated aluminium collectors were incorporated. Comparative analysis with PVDF–NMP cells revealed that the aqueous NMC 622 cell exhibited comparable performance in rate capability tests. Impressively, the aqueous cell surpassed conventional organic cells, demonstrating high cycling stability of 265 cycles at 1C before reaching an 80% state of charge, while organic cells endured only 140 cycles.<sup>141</sup>

The efficacy of PA to prevent corrosion of the aluminium current collector and subsequent crack formation attributed to gas evolution is depicted in Fig. 6, through a comparison of secondary electron images of electrodes before and after cycling with various compositions. The positive impact of PA is also attributed to the formation of the previously mentioned nano-metric layer consisting of transition metal phosphate compounds, particularly Li<sub>3</sub>PO<sub>4</sub>.<sup>87,122,140,173</sup>

Notably, Tolchard *et al.*<sup>142</sup> made a noteworthy observation that deviates from conventional findings. Their investigation revealed that when aqueous processing of NMC 622 cathodes using Na-CMC as binder is executed within relatively short time intervals (45 minutes, as opposed to the more customary 2–3 hours in other studies), the protective layer is inadequately formed, leaving behind electrolyte-soluble residues. These residues, upon interaction with the electrolyte, lead to the development of a thick CEI, resulting in performance degradation. Furthermore, they noted that the electrode formulation using 0.5% PA<sub>NMC 622</sub> outperformed the one with 1.0% PA<sub>NMC 622</sub>—a finding also corroborated by Bichon *et al.*<sup>140</sup> An intriguing solution to mitigate the issue of phosphate residues was identified: conducting electrode washing with ethanol before cycling. This pre-cycling treatment demonstrated a remarkable outcome, showcasing a stable and enhanced cycling performance with a 78% capacity retention after 396 cycles at 1C. The efficacy of this approach highlights the importance of controlling the amount and addition of PA to cathode processing.<sup>142</sup>



Another pH regulator used in the literature is acetic acid, which serves as an effective strategy to prevent the corrosion of the aluminium current collector upon contact with alkaline slurries (pH around 12). Additionally, with increasing amounts of acetic acid, a higher viscosity is observed—a favourable outcome for the formulation of thick-film electrodes. Nevertheless, findings by Zhu *et al.* revealed a noteworthy correlation between the electrochemical performance of NMC 622 cathodes and the pH levels of the electrodes. Specifically, electrodes with lower pH values (7–9) exhibited the poorest performance, attributed to the detrimental impact of excessive acid content leading to a less porous structure and increased cell polarisation. Conversely, slurries without acetic acid (pH 12) demonstrated superior discharge capacities. This was ascribed to enhanced lithium-ion diffusion facilitated by improved electrolyte penetration into the more porous structure. To strike an optimal balance between mitigating aluminium collector corrosion and preserving electrochemical efficiency, the authors recommended maintaining a pH range of 9–10. Furthermore, laser structuring of these electrodes was employed to enhance electrochemical performance, particularly at high C-rates. This structural modification resulted in a 46% increase in capacity at 0.5C for pH 10 structured-electrodes compared to their unstructured counterparts under identical conditions, affirming the efficacy of this technique in promoting lithium-ion diffusion through the provision of additional pathways.<sup>143</sup> Furthermore, when replacing the acetic acid with phosphoric acid for the aqueous processing of thick NMC 622 electrodes with a loading of 34–35 mg cm<sup>-2</sup>, the capacity retention was increased by 57% after 80 cycles at 0.5C for the reference electrode with PVDF binder and by 72% for the laser patterned aqueous electrode using PA as processing additive.<sup>144</sup>

Enhancing the electrochemical performance of water processed NMC 622 cathodes can also be achieved through the application of a silicon oxide coating to the active material. This strategic coating serves to diminish contact with water, consequently minimising the leaching of lithium ions. Moreover, particles of SiO<sub>2</sub>-coated NMC 622 exhibit an increased presence of hydroxyl groups on their surfaces, thereby augmenting particle-to-particle interactions as well as enhancing adhesion to the Na-CMC binder and the current collector. As a result, the cells featuring SiO<sub>2</sub>-coated NMC 622 demonstrated a notable improvement, delivering a capacity of 120 mA h g<sup>-1</sup> after 350 cycles at 1C, compared to their uncoated counterparts, which exhibited a lower capacity of 92 mA h g<sup>-1</sup>. This observed enhancement can be attributed to the protective nature of the inert coating, effectively shielding the active material from electrolyte degradation.<sup>145</sup>

### 3.4 NMC 811

High Ni-content NMCs, exemplified by NMC 811, exhibit an amplified susceptibility to lithium leaching during water processing, leading to a more pronounced increase in pH and consequently diminishing discharge capacities. Various factors contribute to this dissolution phenomenon, including residual

lithium compounds residing on the surface of the active material, the generation of lithium species through interactions with water or CO<sub>2</sub>, and Li<sup>+</sup>/H<sup>+</sup> exchange. The decline in discharge capacity observed during cycling, in comparison to cathodes processed with NMP, suggests that some of the dissolved lithium originates from the active material. In certain instances, the use of lithium foil as an anode can serve as a sufficient lithium source, allowing for the potential relithiation of the active material. Nevertheless, irreversible structural damage may occur during the aqueous processing of nickel-rich active materials, leading to irreversible degradation.<sup>148</sup>

The more pronounced sensitivity of high nickel-content NMCs was studied by Wood *et al.* during a comparative analysis of the water compatibility of various NMCs. Upon subjecting the NMCs to water and analysing the solution using inductively coupled plasma (ICP), negligible dissolutions of transition metals in water were observed. However, a noticeable increase in dissolved lithium was noticed with the increasing nickel content in the NMC structure. Additionally, X-ray photoelectron spectroscopy (XPS) revealed the presence of Li<sub>2</sub>CO<sub>3</sub> on the pristine sample of NMC 811 even without water exposure. Consequently, a portion of the lithium detected by ICP may be attributed to the dissolution of this impurity (Li<sub>2</sub>CO<sub>3</sub>). Furthermore, the other fraction of leached lithium, resulting from the dissolution of lithium in the NMC structure, is believed to re-deposit on the surface after drying, without compromising the initial capacity of the battery. This fact also agrees with XRD results, which did not show any significant bulk structural changes following water processing. As a result, the pouch cells cycled with aqueously processed NMC 811 cathodes using Na-CMC and an acrylic latex as binder demonstrated a comparable initial capacity of 198 mA h g<sup>-1</sup> at 0.1C, with a stable capacity retention of 70% after 1000 cycles at 0.33C (in comparison with 76% for the NMP-processed cells under identical conditions).<sup>78</sup>

Moreover, the increased vulnerability of the NMC 811 active material to water exacerbates cracking issues during the aqueous processing of thick cathodes (with a loading of 5–6 mA h cm<sup>-2</sup>). Utilising Na-CMC and TRD202A as binder, the drying process revealed the occurrence of bubble formation within the coating, giving rise to prominent, large cracks. When the current collector was changed from aluminium to copper foil, the cracks were significantly reduced, underscoring that the primary instigator of bubbles (and subsequent cracking) lay in the hydrogen evolution stemming from the corrosion of the aluminium foil upon exposure to the alkaline slurry. Despite this, residual secondary cracks and pinhole-type defects persisted. Mitigation of these issues was achieved by incorporating 12 wt% of isopropyl alcohol (IPA) as a cosolvent. This addition effectively reduced drying-induced stress by lowering the surface tension of water, thereby precluding the formation of secondary cracks and pinhole-type defects.<sup>84</sup> In addition to the previously discussed approach, Kukay *et al.* explored the impact of introducing phosphoric acid (PA) at varying concentrations (0.5, 1.0, and 1.5 wt%) into the NMC 811 slurry, employing Na-CMC and TRD202A as binders in a 1 : 4 ratio and high loadings (4–6 mA h cm<sup>-2</sup>). Their investigation revealed an improvement





in cycling performance, particularly evident at the 1.0 wt% phosphoric acid concentration that was attributed to the complete mitigation of aluminium corrosion and the development of a  $\text{Li}_3\text{PO}_4$  coating around the active particles, leading to a reduction in cell resistance thanks to its high ionic conductivity. However, it is noteworthy that electrodes lacking phosphoric acid (and consequently experiencing aluminium corrosion) exhibited the highest adhesion strength. The authors explained this phenomenon by pointing to a larger surface area resulting from pits and the infiltration of the slurry, which increased the adhesion between the coating and the current collector.<sup>147</sup> By employing 1 wt% of PA (with respect to slurry solid content) alongside a binder formulation comprising Na-CMC and TRD202A in a 1 : 3 proportion, the aqueous NMC 811 cells exhibited comparable cycling stability to those utilising the conventional PVDF–NMP formulation.<sup>154</sup> Recently, Nagler *et al.* applied a phosphate-based surface coating through a spray-drying process on NMC 811 particles. This innovative approach achieved a dual objective: preventing lithium loss during aqueous processing and enhancing the cycling stability of 3 A h full cells. By reducing the NMC–electrolyte interface area, it effectively minimized undesirable side reactions. Consequently, after 450 cycles at 0.5C, the phosphate-coated NMC 811 cells maintained 94% of their initial capacity, a notable improvement compared to cathodes lacking this protective coating, which exhibited only 85% capacity retention.<sup>159</sup>

Additionally, using PA as a pH regulator for the aqueous processing of NMC 811 cathodes utilising Na-CMC and poly(meth)acrylate (PMA) as binders, Neidhart and coworkers introduced a multilayer coating (ML) technique, to yield defectless thick electrodes with an 8.6 mA h  $\text{cm}^{-2}$  loading, mechanical interconnection between the coating layers, and an even distribution of particles. Notably, a 45% enhancement in adhesion strength of the ML coating to the current collector was discerned compared to its single-layer (SL) counterpart. Concerning electrochemical performance, the most notable improvements were evident at low C rates (0.1C and 0.2C), where the ML coating demonstrated a 20% increase in delivered capacities compared to the SL coating, despite both having identical loading and porosity. At high C-rates (1C), a more moderate capacity increase of 10% was noted, attributed to reduced lithium diffusion in thick electrodes. The improvement was attributed to a diminished charge-transfer resistance and a porosity gradient resulting from the multilayer coating technique. This gradient enlarged the charge transfer sites, facilitating the participation of lithium in the electrochemical reaction, particularly in zones close to the current collector.<sup>151</sup> In a subsequent study, the researchers investigated the implementation of binder gradients, wherein the quantity of PMA binder in the top layer was systematically reduced to 0%, 25%, and 50%. This was compared with their prior research, where the PMA binder constituted 100% in both the bottom and top layers. While no notable changes were observed at low C-rates (below 1C), a distinct enhancement emerged at 1C, with a remarkable 27% and 25% improvement in discharge capacity for the 25%PMA and 50% PMA electrodes, respectively, in comparison to the original ML coating without binder

gradients. Moreover, the capacity retention after 100 cycles at 0.2C exhibited a notable increase from 89% for the no-binder gradient coating to 91% (for 0% PMA and 25% PMA) and 93% for 50% PMA. This improved performance, realised through a reduction in the quantity of insulating binder in the top layer, was attributed to a decrease in electrical resistance. It is worth noting that, in the absence of any binder, a substantial increase in charge transfer resistance occurred due to insufficient bonding ability.<sup>152</sup>

The incorporation of lithium sulphate ( $\text{Li}_2\text{SO}_4$ ) as an additive in the aqueous processing of NMC 811 cathodes also results in the development of a protective coating around the active material, as was observed with PA additives. However, the ineffectiveness of  $\text{Li}_2\text{SO}_4$  in regulating the pH of the slurry leads to corrosion of the aluminium current collector, which is successfully prevented by transitioning to a carbon-coated aluminium collector (CC-Al). Utilising 2 wt%  $\text{Li}_2\text{SO}_4$  in conjunction with CC-Al yields a capacity retention of 84% after 400 cycles at 1C. Conversely, an increase in the amount of  $\text{Li}_2\text{SO}_4$  (5 wt%), which is an electronic insulator, leads to diminished performance due to the elevated resistance of the particle coating.<sup>155</sup>

Kuo *et al.* effectively mitigated voids and cracking issues in their study by introducing poly(acrylic acid) (PAA) as a binder. This strategic application of the weakly acidic PAA resulted in a reduction of the slurry pH to 9, thereby impeding the corrosion of the aluminium current collector. Moreover, the high concentration of carboxyl groups ( $-\text{COOH}$ ) within the PAA structure facilitated their absorption onto the surface of NMC 811 particles, which stabilised the slurry by inducing repulsion among active material particles, preventing undesirable agglomeration. The optimised connectivity between particles and enhanced adhesion had a positive impact on electrochemical reversibility and resulted in low polarisation of the cell. As a result, the cells exhibited an initial discharge capacity of 189.2 mA h  $\text{g}^{-1}$  at 0.2C, attaining a capacity retention of 84.2% after 100 cycles.<sup>88</sup> In a subsequent study, the authors extended their exploration by employing the PAA binder for the aqueous processing of phosphoric acid (PA)-modified NMC 811. This additional step further reduced the slurry pH to approximately 7, although the primary objective was to coat NMC 811 particles with a thin layer of  $\text{Li}_3\text{PO}_4$  to enhance ionic conductivity. However, contrary to expectations, this desired outcome was not observed during cycling. Although the initial capacity at 0.2C was slightly lower compared to their prior work (182.0 mA h  $\text{g}^{-1}$  vs. 189.2 mA h  $\text{g}^{-1}$ ), it recovered to 188.0 mA h  $\text{g}^{-1}$  in the fifth cycle, retaining 99% of this capacity after 100 cycles at 0.2C concerning the first cycle (or 96% in comparison with the fifth cycle). Nonetheless, the authors attributed the improvement more to the presence of PAA binder than the surface modification with PA.<sup>146</sup> The successful outcome of PAA as binder for NMC 811 cathodes was explained by Shunmugasundaram *et al.*,<sup>153</sup> who demonstrated an *in situ* formation of lithium polyacrylate (LiPAA) during aqueous processing (Fig. 7a and b). The weak PAA releases protons in water, promoting lithium leaching over the NMC 811 particles. Concurrently,  $\text{Li}^+$  ions react with  $\text{PAA}^-$ , resulting in the deposition of a layer around the active material, as corroborated by TEM



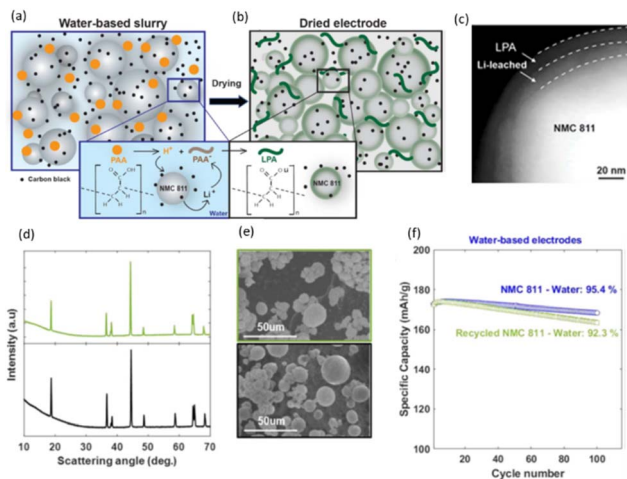


Fig. 7 Schematic representation of the *in situ* formation of lithium polyacrylate during the slurry fabrication (a) and in the final electrode (b). (c) TEM image of the aqueous processed NMC 811 electrode. (d) XRD and (e) SEM images of the pristine (bottom) and recycled (top) NMC 811 cathode material. (f) Galvanostatic cycling of the recycled NMC 811 material in comparison with the pristine one. Reproduced with permission of ref. 153, Copyright 2022, *Journal of Electrochemical Society*.

analysis (Fig. 7c). This approach offers several advantages. Firstly, it mitigates the formation of surface residues such as LiOH or  $\text{Li}_2\text{CO}_3$ . Secondly, as observed by Kuo *et al.*<sup>88</sup> it neutralises the pH to 7 avoiding aluminium corrosion, and also enhances adhesion compared to PVDF electrodes. Most importantly, it facilitates the recycling of the active material through a simple washing and relithiation process to compensate for lithium loss. Fig. 7d and e showcase the XRD and SEM images comparing the recycled NMC 811 with its pristine counterpart. Notably, no discernible differences are evident, underscoring the impressive preservation of the cathode material. Cycling the LiPAA–NMC aqueous cathodes with graphite as the anode achieves an impressive capacity retention of 95% after 100 cycles at 0.2C, while PVDF cathodes demonstrated 97% capacity retention under similar conditions. Subsequent to recycling, the relithiated material exhibits a capacity retention of 92% (Fig. 7f).<sup>153</sup> Boz and coworkers recently reported a significant advancement by successfully upscaling on a pilot line this process of *in situ* formation of LiPAA during the aqueous processing of NMC 811 cathodes.<sup>174</sup>

Another viable strategy to mitigate the formation of cracks and voids resulting from hydrogen evolution due to aluminium current collector corrosion involves substituting the latter with an alternative collector that exhibits resistance to high-pH slurries, such as carbon fabric. The integration of this carbon fabric current collector, coupled with a hydrophilic binder featuring polar groups such as polyacrylonitrile (PAN) effectively improves the wettability across the current collector and retains its initial capacity at 0.5C of  $150 \text{ mA h g}^{-1}$  over 100 cycles.<sup>150</sup>

The integration of styrene-butadiene rubber (SBR) into anodes has gained widespread acceptance alongside the use of sodium carboxymethyl cellulose (Na-CMC). However, the

application of this combination for cathodes presents a distinct challenge due to the susceptibility of the double bond carbon-carbon to oxidation at voltages exceeding 4.2 V, which could make it unsuitable for high-voltage cathodes. Nevertheless, Radloff *et al.* achieved remarkable results, when using this combination of SBR and Na-CMC (in a proportion of 1 and 0.6 wt% of the total electrode composition, respectively) for the aqueous processing of  $\text{LiNi}_{0.83}\text{Co}_{0.12}\text{Mn}_{0.05}\text{O}_2$  (94.4 wt% compared to total solids). The results demonstrated an outstanding rate capability (comparable to PVDF references) and an impressive capacity retention of 84% after 1000 cycles at 1C. The use of a minimal amount of Na-CMC allowed the researchers to employ a reduced quantity of water among their samples, which was attributed to enhanced performance, as a diminished water content limits its availability for lithium leaching to occur. Consequently, it appears that minimising water content and reducing mixing time contribute to enhanced electrochemical performance.<sup>161,175</sup> Moreover, the formulation employing Na-CMC and SBR as binders in a 1:1 ratio, demonstrated successful upscaling from 50 g to 5 kg slurries. This upscaling process facilitated the production of 140 m double-sided cathodes, utilising carbon-coated aluminium as the current collector and phosphoric acid as a pH regulator. The fabricated bilayer pouch cells and 3.5 A h cylindrical cells, featuring the aqueous NMC 811 cathode and graphite-based anodes, exhibited an impressive state of health, with nearly 80% retention after 1000 cycles at 1C.<sup>162</sup> Nevertheless, the performance of the cell based on PVDF-NMP could not be surpassed. One of the reasons proposed by the authors is the elevated moisture content in aqueously processed cathodes compared to PVDF-based ones, particularly considering the hygroscopic nature of water-soluble binders. The residual water may react with the  $\text{LiPF}_6$  salt in the electrolyte, resulting in the formation of hydrofluoric acid (HF), thereby degrading electrochemical performance. This assertion was corroborated through Karl-Fisher titration, revealing a threefold higher moisture content for aqueous cathodes compared to their PVDF-NMP counterparts. The mitigation strategy involved elevating the temperature during the second drying step (from room temperature to 170 °C), with complete removal achievable at temperatures exceeding 150 °C. Surprisingly, the anticipated improvement in capacity with reduced water content was not observed. Contrarily, a reduction in discharge capacity and capacity retention was noted with the increase in the second drying temperature. Remarkably, the optimum performance was achieved by reducing the temperature during the second drying step from 140 °C to 80 °C. This adjustment extended the battery's lifespan before reaching 80% state of health (SOH) from 1000 to 1700 cycles. This phenomenon was explained by the phase reconstruction that occurs on the surface of the NMC 811 active particles, forming a NiO rock-salt layer, which is exacerbated with increasing temperature. This was confirmed by XPS results that showed more  $\text{Ni}^{2+}$  species with rising temperatures.<sup>76</sup> To further enhance the performance of the  $\text{LiNi}_{0.83}\text{Co}_{0.12}\text{Mn}_{0.05}\text{O}_2$  cathodes, the authors shifted from the traditional SBR binder to two alternative binders, namely epoxy and polyisocyanate (ICN). These were synergistically employed



## Tutorial Review

with Na-CMC as a thickening agent in a balanced blend of 1 : 2. Both epoxy and ICN exhibit the ability for chemical crosslinking with Na-CMC, resulting in notable improvements in capacity retention—specifically, an 85% for the epoxy-Na-CMC and an impressive 88% for the ICN-Na-CMC under the same conditions as their previous work (1000 cycles at 1C). Despite the notable achievement of ICN in yielding the highest capacity retention among water-based cathodes, ICN demonstrated a lower discharge capacity than epoxy-based cells at all C-rates, a phenomenon attributed to extensive coverage of the electrode surface, as evidenced by SEM images. This pronounced coverage is hypothesised to impede lithium diffusion within the electrode, thereby influencing overall performance.<sup>72</sup>

Although an effective performance can be achieved through the synergic interaction of SBR and Na-CMC, the biopolymer nature of Na-CMC contrasts with the reliance of SBR production on fossil fuel resources. In pursuit of enhanced sustainability, a random copolymer latex was synthesised based on isobornyl methacrylate (IBOMA) and 2-octyl acrylate (2OA) with a bio content exceeding 70%, which was employed as a binder for NMC 811 cathodes in conjunction with Na-CMC as a thickener and cobinder. The study involved comparing this biobased copolymer latex with the homopolymer latexes of IBOMA and 2OA, representing the hard and soft monomers, respectively. The PolyIBOMA coating exhibited detachment from the current collector due to its insufficient flexibility and adhesion, while the Poly2OA-based electrode displayed numerous cracks attributed to its lack of cohesion. In contrast, the combination of both monomers into the poly(2OA<sub>0.6</sub>-co-IBOMA<sub>0.4</sub>) biobased latex, yielded crack-free electrodes with high peeling strength, ensuring excellent electrode integrity and preventing active material detachment during cycling. The resulting outcome included high specific capacities at elevated C rates, with values of 128 and 100 mA h g<sup>-1</sup> at 3C and 5C, respectively, and a commendable retention capacity of 84% after 90 cycles at 0.5C.<sup>157</sup>

An interesting methodology for the production of ultra-thick water-processed cathodes was devised by Yang and colleagues,<sup>149</sup> incorporating an exceptional 99.5 wt% of NMC 811 in the composition, along with an impressive loading of 511 mg cm<sup>-2</sup>. This innovative approach utilised a gum binder, single-walled carbon nanotubes (SWCNT) as a conductive additive, and employed freeze drying instead of the conventional thermal drying method. The structure of the employed gum binder (Fig. 8a) consisted of xanthan gum, characterised by its double helix structure, and locust bean gum, which featured both hairy and smooth regions. The hydrophilic outer chain of the double helix structure of xanthan gum interacted with the unbranched main structure of locust bean gum. The resulting ultra-thick electrodes, as depicted in Fig. 8b, exhibited a 3D highly aligned columnar structure with open and connected pores, achieved through ice templating during the binder solidification process. This well-organised structure, where the gum binder and SWCNT formed a columnar framework to which NMC 811 particles adhered, facilitated efficient lithium diffusion throughout the ultra-thick electrode. This, in turn, led to a reduction in tortuosity and an increase in electronic

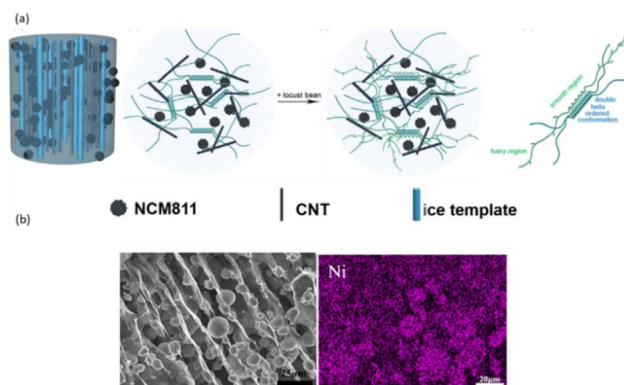


Fig. 8 (a) Schematic representation of the gelation mechanism and directional freeze drying. (b) SEM and EDX images of the aligned structure after freeze drying. Reproduced with permission of ref. 149, Copyright 2021, Wiley.

conductivity. Consequently, the NMC cathode with a loading of 511 mg cm<sup>-2</sup> demonstrated an accessible capacity of 155 mA h g<sup>-1</sup>, retaining an impressive 79% of this capacity after 10 cycles at 0.05C. Remarkably, post-cycling, the cell was disassembled and reconfigured with new electrolyte and lithium foil. The cycling of these new cells displayed a capacity recovery remarkably similar to the initial one, implying that the loss of discharge capacity was not attributed to degradation in the cathode structure, but most likely to the anode and electrolyte.<sup>149</sup> Utilising this freeze-drying technique and the binder composition of SBR and Na-CMC, Wang *et al.* also acquired directional porous structures, demonstrating a discharge capacity of 94 mA h g<sup>-1</sup> at a high C-rate of 10C. Furthermore, the electrodes exhibited a capacity retention of 99.9% after undergoing 100 cycles at a lower rate of 0.5C.<sup>158</sup>

As previously discussed, the utilisation of Na-CMC as a binder has facilitated the exploration of alternative biopolymers distinguished by their natural abundance, adjustability, and cost-effectiveness in contrast to PVDF. Among these alternatives, carrageenan (Carr), categorised as a sulfonated biopolymer, is commercially available with varying sulfonate groups (SO<sub>3</sub><sup>-</sup>)—one, two, or three. Unlike Na-CMC, the sulfonate functionalities in carrageenan structures are inherently occurring, contrasting with the chemical substitution process introducing carboxylic groups in Na-CMC. This intrinsic advantage may lead to a more uniform distribution along the polymer chains, potentially increasing lithium diffusion. In addition to investigating the impact of sulfonate quantity on the aqueous NMC 811 cathode performance, the optimisation of binder content was pursued by reducing it from 5 wt% to 2 wt%. This reduction offers the advantage of increasing the active material in the formulation. Noteworthy is the enhancement in electrochemical performance observed for the reduction of the 3 SO<sub>3</sub><sup>-</sup> carrageenan binder, with a notable increase in capacity from 86.0 to 105.0 mA h g<sup>-1</sup> at 5C when transitioning from 5 wt% to 2 wt%. Conversely, this improvement was not observed for the PVDF electrode when similarly reducing the binder amount, resulting in a capacity loss. Utilising the 2 wt%



formulation, the cells using the  $3\text{SO}_3^-$  carrageenan as binder demonstrated significantly improved dispersion properties, adhesion strength, and preservation of the NMC 811 active material when exposed to water. The higher content of sulfonate groups in the carrageenan structure boosted diffusion kinetics, enhancing the capacity retention from 81% and 87% to 91% when increasing the amount of  $\text{SO}_3^-$  from one and two to three, respectively. Furthermore, the  $3\text{SO}_3^-$  Carr-based electrode also achieved  $133.1 \text{ mA h g}^{-1}$  at 3C and  $105.0 \text{ mA h g}^{-1}$  at 5C, comparable to the organic-based PVDF electrode ( $136.1$  and  $108.7 \text{ mA h g}^{-1}$ , respectively), while providing a more sustainable approach to cathode electrode preparation using a water-soluble, environmentally friendly, and natural polymer.<sup>134</sup> Gan *et al.* introduced a versatile binder for water-based NMC 811 cathodes by crosslinking dextran sulfate sodium (DSS) and LiPAA. The sulfate acid groups and hydrogen bonds of DSS-co-LiPAA were proposed to coordinate with the polar surface of the NMC 811 particles, thereby suppressing transition metal dissolution.<sup>160</sup>

A potential strategy to enhance lithium-ion mobility during cycling involved the utilisation of ionic conductive polymers, such as poly(ionic liquid)s (PILs). Among the extensively studied PILs, poly(diallyldimethylammonium bis(trifluoromethanesulfonyl) imide) (PDADMA-TFSI) based on the pyrrolidinium structure stand out. However, this fluorinated PIL is not water-soluble. Nevertheless, substituting the TFSI<sup>-</sup> with alternative phosphate counter anions yielded two novel water-soluble PILs:

poly(diallyldimethylammonium diethyl phosphate) (PDADMA-DEP) and poly(diallyldimethylammonium dibutyl phosphate) (PDADMA-DBP). These two fluorine-free PDADMA-phosphates exhibited good ionic conductivity at room temperature ( $10^{-6} \text{ S cm}^{-1}$ ) and enhanced wetting properties with the electrolyte. This enhancement facilitated the effective transport of lithium ions throughout the cathode by establishing pathways for their diffusion. Furthermore, these binders demonstrated strong adhesion to the current collector and improved dispersion of active materials. Consequently, upon assembling cells using the PDADMA-phosphates based NMC 811 cathodes with graphite anodes, a discernible improvement in electrochemical performance compared to Na-CMC was observed, which is the aqueous state-of-the-art binder. The PDADMA-DEP cell achieved a discharge capacity of  $101.1 \text{ mA h g}^{-1}$  at a high C-rate (5C) (Fig. 9a), approaching the discharge capacity of PVDF ( $109.2 \text{ mA h g}^{-1}$ ), whereas Na-CMC only delivered  $64.5 \text{ mA h g}^{-1}$ . Furthermore, the capacity retention increased from 81% for Na-CMC to 91% for the PDADMA-phosphates after 90 cycles at 0.5C (Fig. 9b). Examination of SEM images (Fig. 9c–h) of the electrodes post-cycling revealed voids and cracked particles in the Na-CMC electrode, explaining its inferior electrochemical performance. In contrast, PDADMA-DEP and PDADMA-DBP demonstrated a uniform surface with a preserved morphology of NMC 811 particles and the presence of binders as a coating around them, as confirmed by EDX analysis.<sup>116</sup> Soundarrajan *et al.* introduced another pyrrolidinium-based binder derived from poly-1-vinyl-2-pyrrolidinone-crosslinked-prop-2-enoic acid

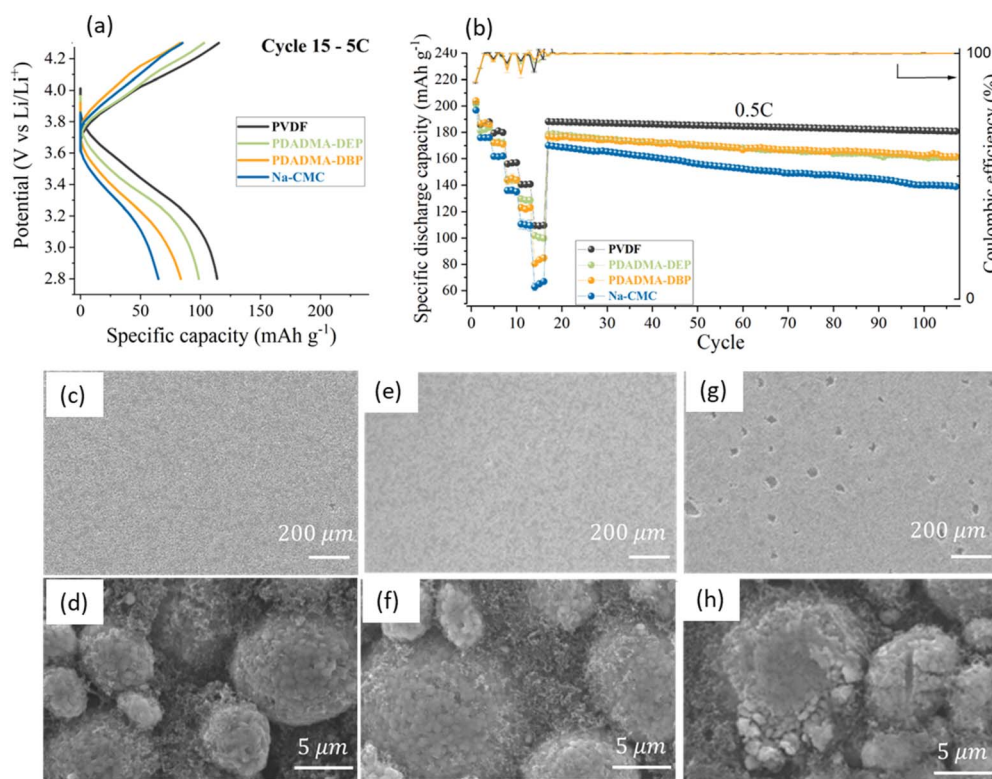


Fig. 9 Galvanostatic cycling of NMC 811-graphite full cells using different binders showing (a) voltage profiles at 5C and (b) C-rate test and cycling performance. SEM images of the aged electrodes (after cycling) with different binders: (c) and (d) PDADMA-DEP, (e) and (f) PDADMA-DBP and (g) and (h) CMC. Reproduced with permission of ref. 116, Copyright 2023, Wiley.



(poly(VPCPEA)) for the fabrication of NMC 811 cathodes, incorporating 70 wt% of active material in the formulation. The robust mechanical strength coupled with multiple polar groups enhanced the mobility of lithium ions within the 3D active functional structure and contributed to reduced polarisation resistance in the aqueous electrodes. Consequently, the poly(VPCPEA) binder facilitated minimal fading, with only a 5.5% decrease observed after 200 cycles at 1C.<sup>156</sup>

## 4 Conclusions & outlook

In this review, a comprehensive overview is conducted of the latest reports on the aqueous processing of NMC active materials using waterborne binders. The focus is on elucidating the advantages, encompassing cost-effectiveness, environmental sustainability, and improved processing conditions. Conventional NMC cathode processing typically involves the use of *N*-methylpyrrolidone (NMP) as the organic solvent and polyvinylidene fluoride (PVDF) as the binder, facilitating the production of mechanically stable and electrochemically efficient electrodes. However, both NMP and fluorine based PVDF are costly and, furthermore, NMP is notorious for its toxicity and teratogenic properties, requiring a complex solvent recovery system, which also increases the cost. The exploration of aqueous processing with water-soluble binders for NMC materials has yielded crucial insights into improving the sustainability of the fabrication of LIBs cathodes. In contrast to conventional PVDF-based electrodes, aqueous binders bring improvements such as enhanced chemical stability and stronger interactions with the rest of the electrode components (*e.g.*, active and conductive material, current collector).

However, the transition from NMP to water in the aqueous processing introduces challenges, including lithium leaching, aluminium corrosion, and electrode cracking, which are exacerbated by the increasing amount of nickel in the composition. Countermeasures include adding a carbon coating layer to the aluminium current collector to avoid its corrosion or adding an acid (*e.g.*, phosphoric acid) to reduce the slurry pH. This latter strategy has been reported to form a protective lithium phosphate layer around the NMC particles, which prevents transition metal dissolution. However, the effect of small amounts of acid on the lithium leaching of these layered cathode materials is still controversial and needs further study. The lithium detected during aqueous processing of NMC materials is reported to be caused by several possible reasons: (i) residual lithium compounds on the cathode surface after synthesis, (ii) lithium surface compounds derived from the reaction with water and CO<sub>2</sub>; or (iii) the lithium leaching that involves a Li<sup>+</sup>/H<sup>+</sup> exchange, accompanied by the formation of LiOH or Li<sub>2</sub>CO<sub>3</sub>. Therefore, it is crucial to meticulously examine the impact of additives, such as phosphoric acid, on diverse cathode active materials when regulating slurry pH. The optimal quantity of the additive for peak performance is interrelated to the structural characteristics of the active material. In addition to performance factors, cost effectiveness and availability are pivotal for practical applications.

The meticulous selection of binders for aqueous NMC cathodes is crucial for achieving optimal battery performance

and sustainability. The criteria encompass a thorough assessment of electrochemical performance, effective binding capability, ion conduction, and suppression of side reactions. The selected binder should demonstrate strong interaction with active materials and conductive particles while minimising parasitic reactions, thereby enhancing battery cycling stability and capacity retention without compromising electrolyte wettability. Equally vital are the mechanical properties, where the binder must prevent material detachment or delamination, address electrode cracks, and exhibit flexibility to accommodate volume changes during battery operation. For this purpose, functional binders containing polar groups have been found to be especially useful. Thermal stability is another critical consideration, requiring resistance to decomposition, volatilization, and melting, as well as the ability to withstand the drying temperature of electrodes during manufacturing.

Emphasizing the necessity to prioritize realistic loadings and binder concentrations in research concerning waterborne electrode production for commercializing LIBs is crucial. While some recent studies have examined novel binders in real-world conditions, a notable portion of research into aqueous processing remains confined to small-scale laboratory setups, typically with low loading electrodes and high binder concentrations. This can lead to misleading conclusions that may not accurately reflect real-world conditions. From an industrial perspective, a primary objective should be to reduce binder content to 3 wt% or lower while maintaining mechanical strength and adhesion, ensuring compatibility with commercial-scale production. Scaling up aqueous processing techniques for industrial applications is a pivotal frontier in the research outlook. Successfully bridging the gap between laboratory-scale success and large-scale manufacturing is essential for the practical implementation of water-soluble binders in commercial battery production. Addressing slurry stability concerns over time and ensuring reproducibility on a larger scale will be paramount to ensuring the successful transition of aqueous processing techniques for practical implementation in large-scale LIB production. Looking ahead, the field of aqueous processing for NMC materials presents exciting opportunities for further advancements and holds promise for revolutionising the electrode fabrication process, contributing to the sustainability and efficiency of lithium-ion batteries.

## Data availability

This review article does not present any new data. Instead, it provides an overview and synthesis of several previously published works. The main highlights from these studies are reported and discussed in the present work. Readers are encouraged to refer to these original publications for detailed data and further information, which can be found in the reference list.

## Author contributions

A. C. R.: writing – original draft, I. d. M., N. C. and M. F.: review & editing. D. M and C. P. G.: review & editing, supervision.



## Conflicts of interest

There are no conflicts to declare.

## Acknowledgements

The authors acknowledge the Australian Research Council (ARC) Centre for Training Centre for Future Energy Storage Technologies (storEnergy) (IC180100049) for funding. Financial support from EU (IONBIKE 2.0 MSCA-SE), Eusko Jaurlaritza (GV-IT1525-22) and MINECO AEI (PID2020-119026GB-I00) is gratefully acknowledged.

## References

- M. Royle, B. Chachuat, B. Xu and E. A. Gibson, *RSC Sustainability*, 2024, **2**, 1337–1349.
- T. Mandel, L. Kranzl, E. Popovski, F. Sensfuß, A. Müller and W. Eichhammer, *Energy Effici.*, 2023, **16**, 22.
- S. Koochi-Fayegh and M. A. Rosen, *J. Energy Storage*, 2020, **27**, 101047.
- Y. Lv, S. Huang, Y. Zhao, S. Roy, X. Lu, Y. Hou and J. Zhang, *Appl. Energy*, 2022, **305**, 117849.
- S. Lee, H. Koo, H. S. Kang, K. H. Oh and K. W. Nam, *Polymers*, 2023, **15**, 1–19.
- A. Perner and J. Vetter, in *Advances in Battery Technologies for Electric Vehicles*, Elsevier, 2015, pp. 173–190.
- A. Murali, S. A. Vallal, M. Sakar, R. Ramesh, M. Devendiran and N. Suthanthira Vanitha, *Adv. Mater. Lett.*, 2022, **12**, 1–9.
- H. Chen, M. Ling, L. Hencz, H. Y. Ling, G. Li, Z. Lin, G. Liu and S. Zhang, *Chem. Rev.*, 2018, **118**, 8936–8982.
- M. Armand, P. Axmann, D. Bresser, M. Copley, K. Edström, C. Ekberg, D. Guyomard, B. Lestriez, P. Novák, M. Petranikova, W. Porcher, S. Trabesinger, M. Wohlfahrt-Mehrens and H. Zhang, *J. Power Sources*, 2020, **479**, 228708.
- N. Lingappan, L. Kong and M. Pecht, *Renewable Sustainable Energy Rev.*, 2021, **147**, 111227.
- P. Das and B. C. Thompson, *Polym. J.*, 2023, **55**, 317–341.
- S. Sudhakaran and T. K. Bijoy, *ACS Appl. Energy Mater.*, 2023, **6**, 11773–11794.
- A. Cholewinski, P. Si, M. Uceda, M. Pope and B. Zhao, *Polymers*, 2021, **13**, 631.
- T. C. Nirmale, B. B. Kale and A. J. Varma, *Int. J. Biol. Macromol.*, 2017, **103**, 1032–1043.
- D. Bresser, D. Buchholz, A. Moretti, A. Varzi and S. Passerini, *Energy Environ. Sci.*, 2018, **11**, 3096–3127.
- J. Li, Y. Lu, T. Yang, D. Ge, D. L. Wood and Z. Li, *iScience*, 2020, **23**, 101081.
- A. Brilloni, F. Poli, G. E. Spina, C. Samorì, E. Guidi, C. Gualandi, M. Maisuradze, M. Giorgetti and F. Soavi, *Electrochim. Acta*, 2022, **418**, 140376.
- W. Dou, M. Zheng, W. Zhang, T. Liu, F. Wang, G. Wan, Y. Liu and X. Tao, *Adv. Funct. Mater.*, 2023, **33**, 1–11.
- H. Huang, C. Liu and Z. Sun, *J. Hazard. Mater.*, 2023, **457**, 131782.
- U. Pal, B. Roy, M. Hasanpoor, H. Ilbeygi, T. Mendes, R. Kerr, L. Vazhapully, C. Song, D. Wang, M. Boot-Handford, M. G. Sceats, M. Forsyth, D. Al-Masri and P. C. Howlett, *Batteries Supercaps*, 2024, **7**, 1–9.
- R. Golmohammadzadeh, Z. Dimachki, W. Bryant, J. Zhang, P. Biniyaz, M. M. Banaszak Holl, C. Pozo-Gonzalo and P. Chakraborty Banerjee, *J. Environ. Manage.*, 2023, **343**, 118205.
- J. Xiao, J. Li and Z. Xu, *J. Hazard. Mater.*, 2017, **338**, 124–131.
- M. Kuenzel, D. Bresser, T. Diemant, D. V. Carvalho, G. T. Kim, R. J. Behm and S. Passerini, *ChemSusChem*, 2018, **11**, 562–573.
- F. Zou and A. Manthiram, *Adv. Energy Mater.*, 2020, **10**, 1–28.
- J. Yoon, J. Lee, H. Kim, J. Kim and H.-J. Jin, *Polymers*, 2024, **16**, 254.
- Y. Ma, J. Ma and G. Cui, *Energy Storage Mater.*, 2019, **20**, 146–175.
- H. J. Noh, S. Youn, C. S. Yoon and Y. K. Sun, *J. Power Sources*, 2013, **233**, 121–130.
- P. S. Salini, S. V. Gopinadh, A. Kalpakasseri, B. John and M. Thelakkattu Devassy, *ACS Sustain. Chem. Eng.*, 2020, **8**, 4003–4025.
- D. Das, S. Manna and S. Puravankara, *Batteries*, 2023, **9**, 193.
- A. M. Pillai, P. S. Salini, B. John and M. T. Devassy, *Energy Fuels*, 2022, **36**, 5063–5087.
- A. Gören, C. M. Costa, M. M. Silva and S. Lanceros-Méndez, *Composites, Part B*, 2015, **83**, 333–345.
- R. Jung, M. Metzger, F. Maglia, C. Stinner and H. A. Gasteiger, *J. Electrochem. Soc.*, 2017, **164**, A1361–A1377.
- T. Dong, P. Mu, S. Zhang, H. Zhang, W. Liu and G. Cui, *Electrochem. Energy Rev.*, 2021, **4**, 545–565.
- J. Li, B. L. Armstrong, J. Kiggans, C. Daniel and D. L. Wood, *Langmuir*, 2012, **28**, 3783–3790.
- K. Y. Cho, Y. Il Kwon, J. R. Youn and Y. S. Song, *Analyst*, 2013, **138**, 2044–2050.
- T. Watanabe, T. Yokokawa, M. Yamada, S. Kurosumi, S. Ugawa, H. Lee, Y. Irii, F. Maki, T. Gunji, J. Wu and F. Matsumoto, *RSC Adv.*, 2021, **11**, 37150–37161.
- X. Zhang, X. Ge, Z. Shen, H. Ma, J. Wang, S. Wang, L. Liu, B. Liu, L. Liu and Y. Zhao, *New J. Chem.*, 2021, **45**, 9846–9855.
- M. Kuenzel, H. Choi, F. Wu, A. Kazzazi, P. Axmann, M. Wohlfahrt-Mehrens, D. Bresser and S. Passerini, *ChemSusChem*, 2020, **13**, 2650–2660.
- S. Pejovnik, R. Dominko, M. Bele, M. Gaberscek and J. Jamnik, *J. Power Sources*, 2008, **184**, 593–597.
- T. W. Kwon, J. W. Choi and A. Coskun, *Chem. Soc. Rev.*, 2018, **47**, 2145–2164.
- S. Tanaka, T. Narutomi, S. Suzuki, A. Nakao, H. Oji and N. Yabuuchi, *J. Power Sources*, 2017, **358**, 121–127.
- Y. B. Wang, Q. Yang, X. Guo, S. Yang, A. Chen, G. J. Liang and C. Y. Zhi, *Rare Met.*, 2022, **41**, 745–761.
- Y. Shi, X. Zhou and G. Yu, *Acc. Chem. Res.*, 2017, **50**, 2642–2652.
- T. Qin, H. Yang, Q. Li, X. Yu and H. Li, *Ind. Chem. Mater.*, 2024, **2**, 191–225.



- 45 I. Kovalenko, B. Zdyrko, A. Magasinski, B. Hertzberg, Z. Milicev, R. Burtovyy, I. Luzinov and G. Yushin, *Science*, 2011, **334**, 75–79.
- 46 R. Gordon, M. Kassar and N. Willenbacher, *ACS Omega*, 2020, **5**, 11455–11465.
- 47 D. Parikh, T. Christensen and J. Li, *J. Power Sources*, 2020, **474**, 228601.
- 48 S. Rajeevan, S. John and S. C. George, *J. Energy Storage*, 2021, **39**, 102654.
- 49 B. Chang, J. Kim, Y. Cho, I. Hwang, M. S. Jung, K. Char, K. T. Lee, K. J. Kim and J. W. Choi, *Adv. Energy Mater.*, 2020, **10**, 1–11.
- 50 Z. Fu, H. L. Feng, X. D. Xiang, M. M. Rao, W. Wu, J. C. Luo, T. T. Chen, Q. P. Hu, A. B. Feng and W. S. Li, *J. Power Sources*, 2014, **261**, 170–174.
- 51 H. K. Park, B. S. Kong and E. S. Oh, *Electrochem. Commun.*, 2011, **13**, 1051–1053.
- 52 H. Isozumi, T. Horiba, K. Kubota, K. Hida, T. Matsuyama, S. Yasuno and S. Komaba, *J. Power Sources*, 2020, **468**, 228332.
- 53 S. Lee, E. Y. Kim, H. Lee and E. S. Oh, *J. Power Sources*, 2014, **269**, 418–423.
- 54 Z. Zhang, T. Zeng, Y. Lai, M. Jia and J. Li, *J. Power Sources*, 2014, **247**, 1–8.
- 55 R. Tatara, T. Umezawa, K. Kubota, T. Horiba, R. Takaishi, K. Hida, T. Matsuyama, S. Yasuno and S. Komaba, *ChemElectroChem*, 2021, **8**, 4345–4352.
- 56 R. Jung, F. Linsenmann, R. Thomas, J. Wandt, S. Solchenbach, F. Maglia, C. Stinner, M. Tromp and H. A. Gasteiger, *J. Electrochem. Soc.*, 2019, **166**, A378–A389.
- 57 N. P. W. Pieczonka, V. Borgel, B. Ziv, N. Leifer, V. Dargel, D. Aurbach, J. H. Kim, Z. Liu, X. Huang, S. A. Krachkovskiy, G. R. Goward, I. Halalay, B. R. Powell and A. Manthiram, *Adv. Energy Mater.*, 2015, **5**, 1501008.
- 58 J. Li, J. Fleetwood, W. B. Hawley and W. Kays, *Chem. Rev.*, 2022, **122**, 903–956.
- 59 Y. Surace, M. Jahn and D. M. Cupid, *Batteries*, 2024, **10**, 100.
- 60 M. J. Lacey, F. Jeschull, K. Edström and D. Brandell, *J. Phys. Chem. C*, 2014, **118**, 25890–25898.
- 61 G. Li, Y. Liao, Z. He, H. Zhou, N. Xu, Y. Lu, G. Sun and W. Li, *Electrochim. Acta*, 2019, **319**, 527–540.
- 62 F. Bigoni, F. De Giorgio, F. Soavi and C. Arbizzani, *J. Electrochem. Soc.*, 2017, **164**, A6171–A6177.
- 63 L. Wang, Y. Fu, V. S. Battaglia and G. Liu, *RSC Adv.*, 2013, **3**, 15022–15027.
- 64 A. Manthiram, *Nat. Commun.*, 2020, **11**, 1–9.
- 65 S. Yang and R. Yang, *Appl. Therm. Eng.*, 2024, **238**, 121991.
- 66 A. Rensmo, E. K. Savidou, I. T. Cousins, X. Hu, S. Schellenberger and J. P. Benskin, *Environ. Sci.: Processes Impacts*, 2023, **25**, 1015–1030.
- 67 D. L. Wood, J. Li and C. Daniel, *J. Power Sources*, 2015, **275**, 234–242.
- 68 X. Zhu, J. C. Roy, X. Li, J. Li and L. Zhang, *Trends Chem.*, 2023, **5**, 393–403.
- 69 N. Susarla, S. Ahmed and D. W. Dees, *J. Power Sources*, 2018, **378**, 660–670.
- 70 R. Sahore, M. Wood, A. Kukay, Z. Du, K. M. Livingston, D. L. Wood and J. Li, *J. Electrochem. Soc.*, 2022, **169**, 040567.
- 71 S. Scott, J. Terreblanche, D. L. Thompson, C. Lei, J. M. Hartley, A. P. Abbott and K. S. Ryder, *J. Phys. Chem. C*, 2022, **126**, 8489–8498.
- 72 S. Radloff, R.-G. Scurtu, M. Hölzle and M. Wohlfahrt-Mehrens, *J. Electrochem. Soc.*, 2022, **169**, 040514.
- 73 S. N. Bryntesen, I. Tolstorebrov, A. M. Svensson, P. Shearing, J. J. Lamb and O. S. Burheim, *Adv. Mater.*, 2023, **4**, 523–541.
- 74 W. B. Hawley, A. Parejiya, Y. Bai, H. M. Meyer, D. L. Wood and J. Li, *J. Power Sources*, 2020, **466**, 228315.
- 75 T. Tanabe, T. Gunji, Y. Honma, K. Miyamoto, T. Tsuda, Y. Mochizuki, S. Kaneko, S. Ugawa, H. Lee, T. Ohsaka and F. Matsumoto, *Electrochim. Acta*, 2017, **224**, 429–438.
- 76 S. Radloff, R.-G. Scurtu, G. Carbonari, M. Hölzle, T. Diemant, M. Bozorgchenani, F. Klein and M. Wohlfahrt-Mehrens, *J. Power Sources*, 2023, **580**, 233314.
- 77 L. Azhari, X. Zhou, B. Sousa, Z. Yang, G. Gao and Y. Wang, *ACS Appl. Mater. Interfaces*, 2020, **12**, 57963–57974.
- 78 M. Wood, J. Li, R. E. Ruther, Z. Du, E. C. Self, H. M. Meyer, C. Daniel, I. Belharouak and D. L. Wood, *Energy Storage Mater.*, 2020, **24**, 188–197.
- 79 M. Hofmann, M. Kapuschinski, U. Guntow and G. A. Giffin, *J. Electrochem. Soc.*, 2020, **167**, 140535.
- 80 I. Hamam, N. Zhang, A. Liu, M. B. Johnson and J. R. Dahn, *J. Electrochem. Soc.*, 2020, **167**, 130521.
- 81 D. Pritzl, T. Teufl, A. T. S. Freiberg, B. Strehle, J. Sicklinger, H. Sommer, P. Hartmann and H. A. Gasteiger, *J. Electrochem. Soc.*, 2019, **166**, A4056–A4066.
- 82 I. Doberdò, N. Löffler, N. Laszczynski, D. Cericola, N. Penazzi, S. Bodoardo, G. T. Kim and S. Passerini, *J. Power Sources*, 2014, **248**, 1000–1006.
- 83 T. Rasheed, M. T. Anwar, A. Naveed and A. Ali, *ChemistrySelect*, 2022, **7**, e202203202.
- 84 R. Sahore, D. L. Wood, A. Kukay, K. M. Grady, J. Li and I. Belharouak, *ACS Sustain. Chem. Eng.*, 2020, **8**, 3162–3169.
- 85 A. Kazzazi, D. Bresser, A. Birrozzi, J. Von Zamory, M. Hekmatfar and S. Passerini, *ACS Appl. Mater. Interfaces*, 2018, **10**, 17214–17222.
- 86 M. Bichon, D. Sotta, N. Dupré, E. De Vito, A. Boulineau, W. Porcher and B. Lestriez, *ACS Appl. Mater. Interfaces*, 2019, **11**, 18331–18341.
- 87 N. Loeffler, G. T. Kim, F. Mueller, T. Diemant, J. K. Kim, R. J. Behm and S. Passerini, *ChemSusChem*, 2016, **9**, 1112–1117.
- 88 J.-H. Kuo and C.-C. Li, *J. Electrochem. Soc.*, 2020, **167**, 100504.
- 89 W. B. Hawley, H. M. Meyer and J. Li, *Electrochim. Acta*, 2021, **380**, 138203.
- 90 K. Kimura, T. Sakamoto, T. Mukai, Y. Ikeuchi, N. Yamashita, K. Onishi, K. Asami and M. Yanagida, *J. Electrochem. Soc.*, 2018, **165**, A16–A20.
- 91 K. Notake, T. Gunji, H. Kokubun, S. Kosemura, Y. Mochizuki, T. Tanabe, S. Kaneko, S. Ugawa, H. Lee and F. Matsumoto, *J. Appl. Electrochem.*, 2016, **46**, 267–278.



- 92 T. Tanabe, Y. Liu, K. Miyamoto, Y. Irii, F. Maki, T. Gunji, S. Kaneko, S. Ugawa, H. Lee, T. Ohsaka and F. Matsumoto, *Electrochim. Acta*, 2017, **258**, 1348–1355.
- 93 T. Watanabe, K. Hirai, F. Ando, S. Kurosumi, S. Ugawa, H. Lee, Y. Irii, F. Maki, T. Gunji, J. Wu, T. Ohsaka and F. Matsumoto, *RSC Adv.*, 2020, **10**, 13642–13654.
- 94 M. Hofmann, F. Nagler, M. Kapuschinski, U. Guntow and G. A. Giffin, *ChemSusChem*, 2020, **13**, 5962–5971.
- 95 Z. Du, K. M. Rollag, J. Li, S. J. An, M. Wood, Y. Sheng, P. P. Mukherjee, C. Daniel and D. L. Wood, *J. Power Sources*, 2017, **354**, 200–206.
- 96 M. A. Sprea, P. Cojocar, L. Magagnin, F. Triulzi and M. Apostolo, *Ind. Eng. Chem. Res.*, 2014, **53**, 9094–9100.
- 97 C. Toigo, M. Singh, B. Gmeiner, M. Biso and K.-H. Pettinger, *J. Electrochem. Soc.*, 2020, **167**, 020514.
- 98 A. Guerfi, M. Kaneko, M. Petitclerc, M. Mori and K. Zaghbi, *J. Power Sources*, 2007, **163**, 1047–1052.
- 99 Z. P. Cai, Y. Liang, W. S. Li, L. D. Xing and Y. H. Liao, *J. Power Sources*, 2009, **189**, 547–551.
- 100 Z. Zhang, T. Zeng, C. Qu, H. Lu, M. Jia, Y. Lai and J. Li, *Electrochim. Acta*, 2012, **80**, 440–444.
- 101 Z. Zhang, T. Zeng, H. Lu, M. Jia, J. Li and Y. Laia, *ECS Electrochem. Lett.*, 2012, **1**, 74–76.
- 102 V. V. N. Phanikumar, V. R. Rikka, B. Das, R. Gopalan, B. V. Appa Rao and R. Prakash, *Ionics*, 2019, **25**, 2549–2561.
- 103 M. Memm, A. Hoffmann and M. Wohlfahrt-Mehrens, *Electrochim. Acta*, 2018, **260**, 664–673.
- 104 A. Vizintin, R. Guterman, J. Schmidt, M. Antonietti and R. Dominko, *Chem. Mater.*, 2018, **30**, 5444–5450.
- 105 J. S. Lee, K. Sakaushi, M. Antonietti and J. Yuan, *RSC Adv.*, 2015, **5**, 85517–85522.
- 106 G. G. Eshetu, D. Mecerreyes, M. Forsyth, H. Zhang and M. Armand, *Mol. Syst. Des. Eng.*, 2019, **4**, 294–309.
- 107 Q. Yang, Z. Zhang, X. G. Sun, Y. S. Hu, H. Xing and S. Dai, *Chem. Soc. Rev.*, 2018, **47**, 2020–2064.
- 108 S. Chauque, F. Y. Oliva, O. R. Cámara and R. M. Torresi, *J. Solid State Electrochem.*, 2018, **22**, 3589–3596.
- 109 M. Forsyth, F. Makhlooghiazad, T. Mendes, N. Goujon, N. Malic, A. Postma, J. Chiefari and P. C. Howlett, *ACS Appl. Energy Mater.*, 2023, **6**, 5074–5080.
- 110 R. Del Olmo, G. Guzmán-González, I. O. Santos-Mendoza, D. Mecerreyes, M. Forsyth and N. Casado, *Batteries Supercaps*, 2023, **6**, e202200519.
- 111 T. A. Ha, H. Li, X. Wang, L. A. O'Dell, M. Forsyth, C. Pozo-Gonzalo and P. C. Howlett, *ACS Appl. Energy Mater.*, 2021, **4**, 434–444.
- 112 V. L. Martins, A. J. R. Rennie, J. Lesowiec, R. M. Torresi and P. J. Hall, *J. Electrochem. Soc.*, 2017, **164**, A3253–A3258.
- 113 J. Liao and Z. Ye, *Electrochim. Acta*, 2018, **259**, 626–636.
- 114 R. Del Olmo, N. Casado, J. L. Olmedo-Martinez, X. Wang and M. Forsyth, *Polymers*, 2020, **12**, 1–18.
- 115 S. Vauthier, M. Alvarez-Tirado, G. Guzmán-González, L. C. Tomé, S. Cotte, L. Castro, A. Guéguen, D. Mecerreyes and N. Casado, *Mater. Today Chem.*, 2023, **27**, 101293.
- 116 A. C. Rolandi, C. Pozo-Gonzalo, I. de Meatza, N. Casado, D. Mecerreyes and M. Forsyth, *Adv. Energy Sustainability Res.*, 2023, **2300149**, 1–11.
- 117 H. Raj and A. Sil, *Ceram. Int.*, 2021, **47**, 34639–34647.
- 118 R. del Olmo, T. C. Mendes, M. Forsyth and N. Casado, *J. Mater. Chem. A*, 2022, **10**, 19777–19786.
- 119 R. Del Olmo, G. Guzmán-González, O. Sanz, M. Forsyth and N. Casado, *Electrochim. Acta*, 2024, **474**, 7.
- 120 L. Ibing, T. Gallasch, P. Schneider, P. Niehoff, A. Hintennach, M. Winter and F. M. Schappacher, *J. Power Sources*, 2019, **423**, 183–191.
- 121 I. Dobryden, C. Montanari, D. Bhattacharjya, J. Aydin and A. Ahniyaz, *Materials*, 2023, **16**, 5553.
- 122 Z. Chen, G. T. Kim, D. Chao, N. Loeffler, M. Copley, J. Lin, Z. Shen and S. Passerini, *J. Power Sources*, 2017, **372**, 180–187.
- 123 N. S. Hochgatterer, M. R. Schweiger, S. Koller, P. R. Raimann, T. Wöhrle, C. Wurm and M. Winter, *Electrochem. Solid-State Lett.*, 2008, **11**, 76–80.
- 124 C. C. Li and Y. S. Lin, *J. Power Sources*, 2012, **220**, 413–421.
- 125 M. H. Ryou, S. Hong, M. Winter, H. Lee and J. W. Choi, *J. Mater. Chem. A*, 2013, **1**, 15224–15229.
- 126 C. P. Jiménez-Gómez and J. A. Cecilia, *Molecules*, 2020, **25**, 3981.
- 127 K. Prasanna, T. Subburaj, Y. N. Jo, W. J. Lee and C. W. Lee, *ACS Appl. Mater. Interfaces*, 2015, **7**, 7884–7890.
- 128 J. He, H. Zhong, J. Wang and L. Zhang, *J. Alloys Compd.*, 2017, **714**, 409–418.
- 129 G. Zhang, B. Qiu, Y. Xia, X. Wang, Q. Gu, Y. Jiang, Z. He and Z. Liu, *J. Power Sources*, 2019, **420**, 29–37.
- 130 D. Versaci, O. D. Apostu, D. Dessantis, J. Amici, C. Francia, M. Minella and S. Bodoardo, *Batteries*, 2023, **9**, 199.
- 131 K. M. Zia, S. Tabasum, M. Nasif, N. Sultan, N. Aslam, A. Noreen and M. Zuber, *Int. J. Biol. Macromol.*, 2017, **96**, 282–301.
- 132 Z. Li, Z. Wan, G. Wu, Z. Wu, X. Zeng, L. Gan, J. Liu, S. Wu, Z. Lin, X. Gao, M. Ling and C. Liang, *Sustainable Mater. Technol.*, 2021, **30**, 1–8.
- 133 T. Kazda, D. Capková, K. Jaššo, A. F. Straková, E. Shembel, A. Markevich and M. Sedlářiková, *Materials*, 2021, **14**, 1–11.
- 134 A. C. Rolandi, C. Pozo-Gonzalo, I. de Meatza, N. Casado, M. Forsyth and D. Mecerreyes, *ACS Appl. Energy Mater.*, 2023, **6**, 8616–8625.
- 135 N. Loeffler, J. Von Zamory, N. Laszczynski, I. Doberdo, G. T. Kim and S. Passerini, *J. Power Sources*, 2014, **248**, 915–922.
- 136 Y. Cui, J. Chen, J. Zhao, Z. Ma, Y. Tan, J. Xue, H. Xu and J. Nan, *J. Electrochem. Soc.*, 2022, **169**, 010513.
- 137 R. Demiryürek, N. Gürbüz, G. Hatipoğlu, M. Er, H. Malkoc, O. Guleryuz, G. Uyar, D. Uzun and M. N. Ateş, *Int. J. Energy Res.*, 2021, **45**, 21182–21194.
- 138 L. Ibing, T. Gallasch, A. Friesen, P. Niehoff, A. Hintennach, M. Winter and M. Börner, *J. Power Sources*, 2020, **475**, 1–9.
- 139 L. Ibing, T. Gallasch, V. Göken, P. Niehoff, M. Winter and M. Börner, *ACS Appl. Energy Mater.*, 2022, **5**, 13155–13160.
- 140 M. Bichon, D. Sotta, E. De Vito, W. Porcher and B. Lestriez, *J. Power Sources*, 2021, **483**, 229097.





- 141 I. de Meatza, I. Urdampilleta, I. Boyano, I. Castrillo, I. Landa-Medrano, S. Sananes-Israel, A. Eguia-Barrio and V. Palomares, *J. Electrochem. Soc.*, 2023, **170**, 010527.
- 142 J. R. Tolchard, P. E. Vullum, B. Arstad and N. P. Wagner, *RSC Sustainability*, 2023, **1**, 378–387.
- 143 P. Zhu, J. Han and W. Pfleging, *Nanomaterials*, 2021, **11**, 1840.
- 144 P. Zhu, V. Trouillet, S. Heißler and W. Pfleging, *J. Energy Storage*, 2023, **66**, 107401.
- 145 J. Sharma, G. Polizos, M. Dixit, C. J. Jafta, D. A. Cullen, Y. Bai, X. Lyu, J. Li and I. Belharouak, *ChemSusChem*, 2023, **16**, e202300350.
- 146 S. Pedaballi and C. C. Li, *J. Power Sources*, 2020, **472**, 228552.
- 147 A. Kukay, R. Sahore, A. Parejiya, W. Blake Hawley, J. Li and D. L. Wood, *J. Colloid Interface Sci.*, 2021, **581**, 635–643.
- 148 M. Hofmann, M. Kapuschinski, U. Guntow and G. A. Giffin, *J. Electrochem. Soc.*, 2020, **167**, 140512.
- 149 S. Yang, C. Zhou, Q. Wang, B. Chen, Y. Zhao, B. Guo, Z. Zhang, X. Gao, R. Chowdhury, H. Wang, C. Lai, N. P. Brandon, B. Wu and X. Liu, *Energy Environ. Mater.*, 2022, **5**, 1332–1339.
- 150 S. Pedaballi and C.-C. Li, *J. Electrochem. Soc.*, 2021, **168**, 120538.
- 151 L. Neidhart, K. Fröhlich, N. Eshraghi, D. Cupid, F. Winter and M. Jahn, *Nanomaterials*, 2022, **12**, 1–15.
- 152 L. Neidhart, K. Fröhlich, F. Winter and M. Jahn, *Batteries*, 2023, **9**, 1–18.
- 153 R. Shunmugasundaram, R. Senthil Arumugam, P. Benedek, M. Yarema, P. Baade and V. Wood, *J. Electrochem. Soc.*, 2022, **169**, 060504.
- 154 F. Wu, M. Kuenzel, T. Diemant, A. Mullaliu, S. Fang, J. K. Kim, H. W. Kim, G. T. Kim and S. Passerini, *Small*, 2022, **18**, 2203874.
- 155 M. Heidebüchel, T. Schultz, T. Placke, M. Winter, N. Koch, R. Schmuck and A. Gomez-Martin, *ChemSusChem*, 2023, **16**, e202202161.
- 156 E. Soundarrajan, L. Prettencia, K. T. Kumar, R. A. Kalaivani and S. Raghu, *J. Energy Storage*, 2023, **73**, 109267.
- 157 A. C. Rolandi, A. Barquero, C. Pozo-Gonzalo, I. de Meatza, N. Casado, M. Forsyth, J. R. Leiza and D. Mecerreyes, *ACS Appl. Polym. Mater.*, 2024, **6**, 1236–1244.
- 158 Y. Wang, Y. Jiang and C. Huang, *Phys. Scr.*, 2023, **98**, 045812.
- 159 F. Nagler, N. Christian, A. Gronbach, F. Stahl, P. Daubinger, A. Flegler, M. Hofmann and G. A. Giffin, *ChemElectroChem*, 2024, **11**, e202300748.
- 160 Q. Gan, N. Qin, H. Guo, F. Zhang, H. Yuan, W. Luo, Z. Li, Y. Li, L. Lu, Z. Xu, L. Wang, J. Lu and Z. Lu, *ACS Energy Lett.*, 2024, **9**, 1562–1571.
- 161 S. Radloff, R.-G. Scurtu, M. Hölzle and M. Wohlfahrt-Mehrens, *J. Electrochem. Soc.*, 2021, **168**, 100506.
- 162 S. Radloff, G. Carbonari, R.-G. Scurtu, M. Hölzle and M. Wohlfahrt-Mehrens, *J. Power Sources*, 2023, **553**, 232253.
- 163 J. Xu, S. L. Chou, Q. F. Gu, H. K. Liu and S. X. Dou, *J. Power Sources*, 2013, **225**, 172–178.
- 164 F. A. Çetinel and W. Bauer, *Bull. Mater. Sci.*, 2014, **37**(7), 1685–1690.
- 165 E. Simonetti, G. Maresca, G. B. Appetecchi, G. T. Kim, N. Loeffler and S. Passerini, *J. Power Sources*, 2016, **331**, 426–434.
- 166 N. Loeffler, G. T. Kim, S. Passerini, C. Gutierrez, I. Cendoya, I. De Meatza, F. Alessandrini and G. B. Appetecchi, *ChemSusChem*, 2017, **10**, 3581–3587.
- 167 D. V. Carvalho, N. Loeffler, M. Hekmatfar, A. Moretti, G. T. Kim and S. Passerini, *Electrochim. Acta*, 2018, **265**, 89–97.
- 168 N. Loeffler, T. Kopel, G.-T. Kim and S. Passerini, *J. Electrochem. Soc.*, 2015, **162**, A2692–A2698.
- 169 H. Zhong, M. Sun, Y. Li, J. He, J. Yang and L. Zhang, *J. Solid State Electrochem.*, 2016, **20**, 1–8.
- 170 W. Bauer, F. A. Çetinel, M. Müller and U. Kaufmann, *Electrochim. Acta*, 2019, **317**, 112–119.
- 171 J. T. Li, Z. Y. Wu, Y. Q. Lu, Y. Zhou, Q. Sen Huang, L. Huang and S. G. Sun, *Adv. Energy Mater.*, 2017, **7**, 1–30.
- 172 S. N. Bryntesen, P. H. Finne, A. M. Svensson, P. R. Shearing, N. Tolstik, I. T. Sorokina, J. Vinje, J. J. Lamb and O. S. Burheim, *J. Mater. Chem. A*, 2023, **11**, 6483–6502.
- 173 C. H. Jo, D. H. Cho, H. J. Noh, H. Yashiro, Y. K. Sun and S. T. Myung, *Nano Res.*, 2015, **8**, 1464–1479.
- 174 B. Boz, K. Fröhlich, L. Neidhart, P. Molaiyan, G. Bertoni, M. Ricci, F. De Boni, M. Vuksanovic, M. Romio, K. Whitmore and M. Jahn, *Chempluschem*, 2024, e202400195, DOI: [10.1002/cplu.202400195](https://doi.org/10.1002/cplu.202400195).
- 175 F. Nagler, N. Christian, P. Daubinger, A. Flegler, M. Hofmann and G. A. Giffin, *J. Power Sources Adv.*, 2023, **24**, 100131.

